The Red Clump Stars as a Distance Indicator: Review and Application

by

Camaren Peter

Thesis submitted in fulfillment of an MSc degree at the University of Cape Town, South Africa. This research project was conducted under the supervision of Dr John Menzies at the South African Astronomical Observatory and Professor Brian Warner at UCT.

Abstract

The intention of this project was primarily to determine the distance to the Galactic Centre using a new technique pioneered by Paczynski and Stanek (1998) that uses the red clump stars as a standard candle. This was made possible by the large numbers of stars simultaneously observed by the OGLE microlensing project which yields well defined red clump structures in their colour magnitude diagrams. We have used data obtained at Sutherland in July 1997, in collaboration with the PLANET microlensing project. It was hoped that the observation of a number of lensing events occurring in fields in the Galactic Bulge region would reveal information about the Galactic structure in that region and perhaps yield information about the lens masses. The red clump technique is reviewed and applied to several 3×3 arcmin fields observed at low galactic latitude and longitude in the Galactic Bulge. The derived distances to the fields show consistency with the E2 bar model proposed by Stanek, and indicate that the distance from our sun to the Galactic Centre is 7.97± 0.4 kpc. Furthermore, an attempt is made to apply the derived individual distance to each field to calculate the possible lens mass associated with each event.

Acknowledgements

"In ambition gravitates the subjectivity of being ..."

Thabani Gumede

I would like to extend my deepest gratitude to the following people:

- **Dr John Menzies**, my supervisor. Thank you for the patient guidance and inspirational conversation which often extended far beyond the realm of astronomy and taught me the value of rigourous thought and analysis in every aspect of life. Working with you has enlightened me in many ways.
- **Prof Brian Warner** and **Prof Don Kurtz** for teaching me the basics of astronomy. The lectures were inspiring because of the enthusiasm and dedication you displayed for researching and teaching astronomy.
- **Prof Michael Feast**, for helpful and informative discussions about the distance scale and the peculiarities of evolution of stars up the red giant branch.
- **Dr Darragh O'Donoghue**, for his patience in teaching me Fortran which enabled me to conduct my data analysis with ease.
- **Dr K Z Stanek and Dr B Paczynski**, for replying almost instantly to various electronic mail inquiries with keen and encouraging interest.
- **Dr Patricia Whitelock**, for the earnest and supportive interest in my academic success.
- **Ethleen Lastovica**, the SAAO librarian, for her invaluable assistance.
- **Veronique Kazie**, for providing thorough and instantaneous help with every computer problem I encountered.
- To all the students at SAAO who form a good support base both socially and academically.

- The numerous SAAO staff members who were always helpful and considerate when approached.
- My family and friends, who have shown interest and given encouragement when it was most needed.
- **Thembi Russell**, for all the love and confidence you inspired by your very nature.

A Dedication:

I dedicate this thesis to my beautiful continent Africa, which has fed me and grown me. It is my greatest wish for us to develop a powerful academic and political culture which is truly African. To this end, may we one day abandon violent conflict and recognise our common humanity.

Chapter One: Introduction

In astronomy, distances to objects are found using a variety of techniques. However, not all of these techniques show consistency when they are compared. Indeed, some of the distances are found to be so different that the search for an accurate technique to estimate distances continues. The vast number of stars observed in the microlensing surveys makes it possible for us to investigate the use of the red clump as a standard candle. Its use may be fundamental to re-estimating the distance to the Galactic Centre.

1.1 The Distance to the Galactic Centre

The distance R_o to the centre of our Galaxy is of great importance to astronomy. It acts as a scale factor to physical properties of the Galaxy and the Universe (Reid, 1993):

- All distances determined by observing radial velocities and using a rotation model of the Galaxy are directly proportional to R_o.
- Estimates of the gravitational and luminous mass of the Galaxy also scale with R_o.
- Similarly masses and luminosities of objects such as giant molecular clouds and the non-thermal source at the Galactic Centre depend on R_o.
- In addition, since R_o is used to calibrate extragalactic distances, R_o is related to the Hubble constant.

Historically, the distances to nearby stars were calculated and used to calibrate luminosities. Thereafter R_o was measured from the spatial distribution of stars and globular clusters. Recently, attempts at measuring the distance to the centre of the Galaxy directly have been made by analysing the proper motions of H_2O masers which occur at the periphery of newly formed massive stars; however, large uncertainties hamper attempts to constrain R_o properly.

Secondary measurements of the distance to the centre of the Galaxy include;

- The above-mentioned technique (employed by Shapley) where the centroid of the distribution of globular clusters that are assumed to be symmetrically distributed around the Galactic Centre is located.
- Investigating the metallicity of globular clusters. These seemed to show a decrease in metallicity outwards from the Galactic Centre. If the globular cluster distribution is axially symmetric about the axis of Galactic rotation then an estimate of R_o can be obtained by adjusting its value until there is no correlation between the galactocentric azimuth and the cluster metallicity.
- The observation of RR Lyrae variable stars through Baade's window of low extinction. Since the mean magnitude of the RR Lyrae variables and the horizontal branch are nearly identical, globular cluster distances are correlated with those of RR Lyrae variables. However, the metallicity dependence of the mean magnitude of the RR Lyrae variables is a disputed issue. Some studies claim that no metallicity dependence is revealed by analysing groups of different metallicities, while others argue for a range of up to 0.8 mag.

As a result of the controversy surrounding metallicity and extinction effects upon stars of various types (e.g. Cepheids, RR Lyraes, Red Clump Stars ...) in the galactic bulge and disk, observers have looked to infrared observations to circumvent or reduce the effects of metallicity and extinction in their observations. In the infrared:

- The mean magnitude of a star may be determined more accurately from a smaller number of observations. This is because the light curves in the instability strip have smaller amplitudes in the infrared.

- Absorption corrections in the infrared are considerably smaller than in the visual.

- In addition, stellar atmospheric opacities are smaller at longer wavelengths implying that metallicity corrections to absolute magnitudes are smaller in the infrared.

Astronomical observations are conducted by collecting radiation in different regions of the electromagnetic spectrum. In order to give meaning to the amount of flux radiating from the surface of the star it is important to know, to good accuracy, how far away from the star the observer is. This in turn has repercussions on the amount of insight we have into how the star is functioning at a physical level.

Astronomers are concerned with luminosity, and a logarithmic measure of it, described as a magnitude. Apparent magnitudes refer to energies received above the earths atmosphere, and are described by the equation

1.1 $m = const - 2.5 \log l_s$, where

m - magnitude

l_s - stellar luminosity (total light output).

The absolute magnitude describes the energy received at ten parsecs away from the star

1.2 $M = m - 5 \log(\frac{d}{10})$, where

d - distance in parsecs where one parsec is the equivalent of 3.26 light years.

Knowing the distance to a star accurately gives us a better idea of the luminosity of the star. The luminosity and the effective temperature are graphed into what is known as a Hertzprung-Russell diagram (hereafter HR diagram), a fundamental diagram in astronomy.

1.2 The Red Clump Stars

The Hertzprung-Russell diagram features many consistent structures resulting from the evolution of stars of different masses. On the HR diagram about ninety percent of a stars total lifetime is spent burning hydrogen in the main sequence phase of evolution. This is a phase in which the star is fusing hydrogen into helium in its core. Main sequence stars of greater mass exhibit higher luminosities and spend less time on the main sequence. One may describe the evolution off the main sequence as follows (Iben, Tayler, Bohm-Vitense):

The mass of the core plays an important role in determining the way in which the star evolves. For low mass stars we have relatively little or no convection in the core. The cores are not mixed for this reason. Thus, hydrogen is depleted first in the central region of helium burning. In an electron degenerate core pressure is not a function of temperature. For this reason, the rise in temperature does not result in an increase in pressure within the core. The shell source forms, and the core starts contracting long before it is anywhere near the Schonberg-Chandrasekhar limit. At this limit, the pressure in the isothermal core is unable to sustain the pressure of the outer regions of the star and a rapid collapse ensues. This occurs during the evolution of more massive stars. The movement away from the main sequence is less rapid for low mass stars, and the onset of degeneracy and an outer convection zone occur sooner than for high mass stars. The slow evolution off the main sequence is an observed phenomenon in the HR diagrams of globular clusters (i.e. no gap exists). Hydrogen becomes depleted in the core and energy production moves to a region where hydrogen is more abundant and the temperature is high. Firstly, a shell source develops around the rim of the helium core. The shell burns and thickens and soon becomes the main energy source in the star, producing more energy than the core. Hydrogen is available to it in the envelope above and the shell starts to burn outwards. Material in the envelope above it is heated and recedes in front of the shell, and the star expands. The shell narrows, and towards the end of this phase the envelope starts to become convective. Convection becomes increasingly

dominant as a mode of energy transport and mixing results. The dominant source of opacity in the region between the outer edge of the convective envelope and the surface of the star is the H^- ion. The opacity decreases with decreasing temperature in the photosphere, and this favours a larger energy flow to the surface of the star. Thus, the blanketing effect of the stellar envelope decreases as the mass of the convective envelope increases and the star's luminosity increases as more radiation is able to reach the surface. Envelope convection dominates while the shell burns its way outward through the star. At the tip of the red giant branch (hereafter RGB) the core has reached temperatures high enough to start fusing helium into carbon. The `helium flash' occurs. This is the violent onset of would result in expansion and thus cooling. The temperature continues to rise until it is high enough to remove degeneracy. In this scenario, the material will expand in an explosive manner due to the runaway release of nuclear energy. This violent helium flash for low mass stars complicates the study of stellar evolution, in particular, the ability of solar models to describe it. In any event, it is after the helium flash that the star settles into the core helium-burning phase of evolution. It is the metal rich equivalent of these core helium-burning stars that form the red clump just below the tip of the RGB in the HR diagram. The upper mass limit for developing an electron degenerate core and entering this phase of evolution is about 2.4 $M_\odot$ for solar abundances (Girardi et al 1998, Sweigart et al 1990). For stars of low metallicity, we see a horizontal branch located at fainter magnitudes than the clump stars. These stars have lost more mass in the helium flash phase. These stars exhibit an almost constant luminosity in this phase. For masses slightly above this limit they may burn helium in a weakly degenerate core for which the RGB phase is much shorter, and will have a luminosity of value about 0.4 mag below the clump of lower mass stars.

It is these stars, which make up the red clump, and which we consider as standard candles. The large numbers of observed red clump stars enables us to reduce the statistical error significantly. In addition, in a given stellar system (where all stars are at about the same distance) the clump stars have a relatively small range in apparent brightness and the mean absolute brightness does not vary much between different systems.

1.3 Description of Thesis Contents

Chapter two is mainly a review of the literature surrounding the red clump distance technique. It contains a discussion of the method employed to use the red clump stars to calculate astronomical distances, and a review of the consequent debate surrounding the validity of its use.

Chapter three contains a description of the observed data and the methods employed to transform the data onto the standard system. The setting of the zero point is explained and performed. This is then applied to the data and colour-magnitude diagrams are presented. In addition, the method used to account for reddening and extinction is discussed and performed and the resulting colour magnitude diagrams are presented.

In Chapter four a discussion of how we modified the red clump distance calculation technique for our use is presented and the statistical error associated with the distance calculations are evaluated. The results of the distance calculations are then presented and tentatively applied to the proposed bar structure of the Galactic Bulge.

In Chapter five, an attempt is made to use our results to investigate the microlensing events associated with each observed Bulge field. A method for ascertaining the spectral type of the source stars and the mass limits for the lenses is discussed and applied to our results. In this latter section of the chapter the emphasis is placed on the methodology rather than the crude results obtained.

Chapter six is the concluding chapter and presents a short discussion of the usefulness of the work presented in this thesis.

Chapter Two: A Review of the Red Clump as a Standard Candle

2.1 Introduction

In all secondary distance measurements the star that is observed must be compared with stars of the same type for which we know, to good accuracy, the absolute magnitudes and consequently the distances to these objects. The Hipparcos satellite has provided us with a catalogue of stars containing many clump stars with parallaxes better than ten percent accuracy. These are stars in our solar neighbourhood; and therefore certain factors are introduced from which our distance estimate suffers, namely, (Paczynski & Stanek, 1998: hereafter P&S):

- The accuracy is dependent on the accuracy of known stars in the catalogue. Nevertheless there is a large sample of stars in the Hipparcos catalogue with parallax errors of at least ten percent..

- Interstellar extinction must be separately determined near the Galactic Centre and in the solar neighbourhood so that comparison can be made between stars from two different regions of the Galaxy.

- Stars in our solar neighbourhood may differ from Bulge stars in chemical composition, age and mass.

- If we have a small number of objects as we often do with Cepheids and RR Lyraes, then a large statistical error results. The large statistical error often associated with small numbers of observed standard candles may be greatly reduced by comparing clump stars, as they occur in great numbers in most stellar populations.

2.2 The Method

The probability of observing a gravitational microlensing event is one in a million. For this reason, microlensing surveys cover a large number of stars. As a by-product of these extensive surveys we have photometry for thousands of stars which may be presented in colour-magnitude diagrams.

Investigation of the clump regions of both Hipparcos stars and the Bulge stars reveal that the mean infrared magnitudes M_I are independent of the (V-I) colour index (P&S). This was taken to indicate that M_I is independent of age and chemical composition and thus may be used as a standard candle. It was expected that a comparison between the Bulge stars in Baade's window and the solar neighbourhood stars measured by Hipparcos could safely be made. In addition, P&S claim that the models of Seidel, Demarque and Weinberg (1987, hereafter SDW) predict that absolute luminosity depends weakly on age and chemical composition. This is a contentious issue. Girardi et al (1998) claim that clump stars of different masses and metallicites are shown in SDW to have luminosities differing by up to 0.5 magnitudes. While this is true, it is worth mentioning that the clumps generated with higher metallicity (Z=0.01) all exhibit a spread in width less than 0.2 mag. It is only the clumps generated with much lower metallicity (Z=0.001) that actually exhibit a spread as large as 0.5 mag. Now, in the context of stellar evolution theory the red clump is populated with low mass stars of high metallicity while the horizontal branch situated below the red clump structure is populated with low mass stars of lower metallicity. It could well be that the results of the low metallicity model (Z=0.001) was ignored by P&S because it was felt that it was not representative of the red clump stars (which are metal rich) but rather was representative of the horizontal branch stars. In any event, it was thus purely the observed M_I independence of colour that prompted the use of red clump stars as standard candles.

Stanek (1996) constructed an extinction map for a 40×40 arcmin region of Baade's window. This was performed using a method proposed by Wozniak and Stanek (1996) to investigate interstellar extinction that involved using two-band photometry of the red clump stars to construct the reddening curve.

The extinction maps of Stanek (1996) for Baade's window are used to correct the colour-magnitude (CM) diagram. The selected clump region is then binned into a histogram showing the number of stars in each magnitude range. This histogram is fitted with a function

$$2.1 \quad n(I_o) = a + b(I_0 - I_{o,m}) + \frac{N_{RC}}{\sigma_{RC}\sqrt{2\pi}} \exp[-\frac{1}{2}(\frac{I_o - I_{o,m}}{\sigma_{RC}})^2] ,$$

where the first two terms are meant to take into account the 'background' of red giant stars in the HR diagram, and where;

σ_{RC} =0.28 - OGLE clump

σ_{RC} =0.24 - Hipparcos clump (in magnitudes).

Ranges:

$0.8 \leq (V-I)_o < 1.25$ - Baade's Window

$0.8 \leq (V-I)_o < 1.25$ - Hipparcos (in magnitudes).

In their (P&S) rough first approximation they derive $I_{o,m}$ =14.323±0.009, with $M_{I,m}$=-0.185±0.0116, and deduce a distance modulus of $(m-M)$ =14.508±0.019, corresponding to a distance of 7.97±0.08kpc.

The above-mentioned P&S calculation comes from Hipparcos stars with parallaxes of accuracy better than 10 percent. The calculations were then repeated using stars from the Hipparcos catalogue known to within five percent parallax error, and a similar dispersion and mean absolute

magnitude were obtained. This showed that the use of less accurate data does not introduce a significant bias.

A distance bias is introduced by using Hipparcos stars which are intrinsically brighter and can thus be measured out to larger distances. Hipparcos stars are chosen as having parallax errors less than 10 percent. Therefore the accuracy of a Hipparcos measurement depends on the apparent brightness the star. Hence the intrinsically bright Hipparcos stars in the sample used come from a larger volume of space than the intrinsically faint ones and the resulting mean intrinsic luminosity of the sample is brighter than it would be for a volume limited sample. Thus, there are more bright stars in the Hipparcos sample than in the OGLE data that introduces a shift into the location of the Gaussian peak corresponding to the b coefficient in equation (2.1). The number of Hipparcos stars in each bin was then weighted by a factor

$$2.2 \qquad f = \frac{a_{BW} + b_{BW} M_I}{a_H + b_H M_I}$$

that normalized the fit and yielded a value $M_{I,m}$=-0.125±0.019 for absolute mean clump magnitude corrected for distance bias.

The interstellar extinction for the Hipparcos stars had to be calculated. They selected a sub-sample of 228 Hipparcos stars with distance less than 70 parsec and determined the parameters of the best fit to the luminosity function equation (1), correcting for distance bias, and ascertained that $M_{I,m}$=-0.192±0.023 and σ_{RC}=0.208 for the nearby stars with average distance coming out as 50 pc. This was compared to 437 Hipparcos clump giants further than 70 pc away and it was found that $M_{I,m}$=-0.094±0.027, σ_{RC}=0.234 and the average distance was 106 pc. The more distant stars were fainter by 0.098 mag while their difference in distance was 56 pc. This is assumed to be due to interstellar extinction. They extrapolate back to d=0 (i.e to 0 extinction) and obtain $M_{I_o,m}$=-0.279 and their final estimate is 0.088 magnitude brighter than the original estimate. They take this to be a crudely estimated indication of what the systematic error might be. They do

mention however, that the differential extinction used is significantly higher than that which has previously been determined.

They then investigate the Galactic Bar asymmetry and take into account that the observed centroid of distribution for red clump giants corresponding to the point of highest space density of red clump stars in the direction of Baade's window is closer than the Galactic Centre. Also, more stars are observed on the far side than on the near side of the Bar due to the increase with distance of the volume of the observed solid angle, implying that the observed centroid is shifted to a somewhat larger distance than the location of the highest space density of the Bar stars. These two effects oppose one another and the E2 bar model of Stanek et al (1997), was used to calculate them. It was found ,that the real distance to the centre of the Galaxy would be larger by 0.02 mag than that obtained from the centroid distribution. The error in the zero point of extinction maps contributes the largest error, 0.05 mag (Gould et al 1997, Alcock et al 1997). The corrected distance is eventually thought to be R_o=8.4±0.4kpc with distance modulus, 14.62±0.10. This value has since been corrected to 8.2±0.3kpc by Stanek and Garnarvich (1998); where they corrected for the zero point of the extinction map for Baade's Window established by Stanek (1996).

Of course the extent of the possible systematic error that age and chemical composition would introduce into the distance estimate is unknown. The colour differences between Bulge and solar neighbourhood clump giants suggest that there are differences, although consensus on what those actually are has not been reached (Paczynski, 1998).

2.3 Consequent General Results and Debate

2.3.1 Introduction

The red clump technique has had some success. In particular, the distance calculated to the Bulge (P&S) and to M31 (Stanek and Garnarvich, 1998) was in agreement with distances calculated by other reliable distance calibrators. Using the red clump technique outlined above, Udalski et al (1998) obtained distances to four fields in both the Large Magellanic Cloud (LMC) and the Small

Magellanic Cloud (SMC), for which they found distance moduli 0.4 magnitudes smaller than the generally accepted values. This corresponds to the Magellanic Clouds being fifteen percent closer than generally accepted. It was assumed that a red clump feature, the vertical red clump (VRC), first noted by Zaritsky and Lin (1997) was taken to be an evolutionary feature rather than a foreground population, which would explain the brighter magnitudes calculated. This conclusion was bolstered by Beaulieu and Sackett (1997) who showed that this feature had to be evolutionary since;

- Its presence was detected in all LMC fields
- It agreed in location with that of blue loops in the isochrones of intermediate age red clump stars with the age and metallicity of the LMC.
- It was also shown to be present in the Hipparcos CMD for the solar neighbourhood, where an intervening population cannot be invoked.

Seeing that the mean metallicities of stars in the Magellanic Clouds exhibit lower mean metallicities than stars occupying the solar neighbourhood and the Bulge, it was suspected that chemical composition may indeed have a significant effect on the mean clump magnitude.

Metallicity

An increase in metallicity is expected to yield a redder colour. There are several reasons for this. First, a higher metallicity in an atmosphere corresponds to an increase in absorption and a corresponding increase in opacity. This would result in an increase of the stellar radius corresponding to a lowering of the effective temperature. This can be interpreted as a cooling effect that would redden the observed radiation. Secondly, the effect of line blanketing associated with an increased opacity would result in the observed radiation being emitted from cooler layers that would also demonstrate reddening. Both effects predict a reddening, so we would expect metal rich stars to be redder. This is indeed an effect displayed by stellar evolution models.

Helium

The effect of helium mixing from within the hydrogen shell into the envelope due to internal rotation has been shown (according to solar models) to result in increased mass loss and higher luminosities in the RGB phase and the horizontal branch phase, resulting in a bluer and brighter horizontal branch (Sweigart, 1997). This may be falsely interpreted as an age effect, reducing the ages of clusters determined from the luminosity difference between the horizontal branch and the main sequence turnoff. In addition, the mixing of helium might result in a larger RR Lyrae period shift and a steeper RR Lyrae luminosity-metallicity relation if more mixing occurs at low luminosities.

The observation of super oxygen-poor stars near the RGB tip in M31 (Kraft et al 1993, 1997) indicates that red giants of low mass are indeed capable of mixing nuclear-processed material from the vicinity of the hydrogen shell out to the surface (Kraft, 1994). It has been shown (Langer, Hoffman, & Sneden, 1993) that aluminium can be produced in low mass red giants via proton capture on Mg but that this process seems to occur only within the hydrogen shell (Langer & Hoffman 1995; Cavallo, Sweigart & Bell, 1996, 1997). It stands to reason then that any mixing process that dredges up Al will also dredge up helium from the shell. Variations of Al have indeed been observed by Norris & Da Costa (1995), and in Kraft et al (1997). This may indeed have consequences for the red clump stars as well, because any mixing of helium into the envelope while stars are evolving along the red giant branch will have consequences for the red giant branch clump.

The approach of the model-based investigations which will be described shortly was to make investigations into the effects of age, metallicity and helium content of the clump stars, and in turn, to try to explain how a mean I magnitude that is constant over the (V-I) range of the clump but variable in its actual value of mean magnitude could be reproduced. These investigations have reproduced and yielded plausible explanations for red clump morphology, indeed even for the VRC.

Table 1: The results reproduced in this table appear in Cole (1998) and show the shifts in mean red clump I-band absolute magnitude as a function of mass and metallicity as computed from the models of Seidel, Demarque and Weinberg (1987).

Mass	Z	$\delta M_I^o(mag)$
1.7	0.02	-0.17
...	0.01	-0.27
...	0.004	-0.42
...	0.001	-0.65
1.5	0.02	-0.13
...	0.01	-0.23
...	0.004	-0.35
...	0.001	-0.43
1.2	0.02	-0.00
...	0.01	-0.10
...	0.004	-0.20
...	0.001	-0.32
1.00	0.02	+0.05
...	0.01	-0.03
...	0.004	-0.07
...	0.001	-0.10

2.3.2 Model based Investigations

Cole investigates the luminosity dependence of the red clump on age and metallicity, finding that an uncertainty of up to 0.6 mag in the mean absolute magnitude can result. He examined the theoretical red clump models of Seidel et al (1987a) which contained evolutionary tracks for masses between 0.74 and 1.7 solar masses and metallicities ranging Z= 0.001, 0.004, 0.01, 0.02. Relative shifts between $M_I(local)$ and the mean luminosity of the clumps were defined for each track by finding points in the track where evolution was slowest and hence more likely to be observed. Their best-fit result for the shift was $\Delta M_{Io} = (0.021 \pm 0.07)[\frac{Fe}{H}]$.

Tabulated in Table 1 are the theoretical results obtained. He asserts that clump magnitude is almost independent of mass for stars less than 1.2 $M_{\odot}$ but can still vary with metal abundance. Two different types of star formation history are investigated; that of Holtzmann et al (1997), where 73 percent of the clump is produced with a mean metallicity Z=0.001 between 2 and 10 Gyr ago, and the rest derives from a 1-2 Gyr old population having a higher metallicity Z=0.008, and, the 'burstlike' star formation history of Vallenari et al (1996) where 44 percent is produced with Z=0.04 between 2 and 10 Gyr ago, and 56 percent having Z=0.008 being 1-2 Gyr old.

The Holtzmann-like star formation history was thought to be more compatible with the LMC, seeing that Stanek, Zaritsky & Harris (1998) point out that a Vallenari-type star formation history would result in a large dispersion in clump properties, which is not observed. A colour shift indicated between the solar metallicity clump and the LMC prompted a 0.04 mag shift.

For the SMC where the star formation history was considered to be less constrained, a mean value between a constant and burst scenario was adopted. They conclude that distance moduli are

2.3 $(m-M)_{LMC} = 18.36 \pm 0.05(random) \pm 0.12(systematic)$, and

2.4 $(m-M)_{LMC} = 18.82 \pm 0.07(random) \pm 0.13(systematic)$;

bringing the distance moduli into closer agreement with Cepheid distances, the best value for which is 18.94±0.04 and 18.50±0.10 (Laney and Stobie, 1994) for the SMC and the LMC respectively.

Cole estimates that the variations of core mass Mc and Y and Z is likely to result in a shift ΔM_{I_0} less than 0.15 mag in most cases and less than 0.10 mag for the considered cases. This estimate is made from the tabulations of Sweigart and Gross (1978). For populations older than 6 Gyr, this effect is of the correct order to erase the metallicity effect, while for the younger populations it will reduce the metallicity effect.

Cole claims that this explains why different degrees of accuracy, in comparison to other distance indicators, were obtained between the older Galactic Bulge population and the younger Magellanic Clouds. Cole concludes that the red clump method can be applied confidently to stellar populations known to be older than 6 Gyr, while for younger populations M_{Io} will be brighter than $M_{Io}(local)$, and will have to be corrected by up to as much as several tenths of a magnitude. It was at this stage of the debate that the red clump was proclaimed to be a non-standard candle.

More recently, Girardi et al (1998) showed that using a population synthesis approach the constancy of M_I with colour for the local Hipparcos sample could indeed be reproduced while M_I could still depend on metallicity and not be constant among different populations. In addition, their models predict a secondary clump structure about 0.3 mag below the bluest extremity of the red clump, formed by stars slightly heavier than the maximum mass for developing degenerate helium cores. This secondary clump is identifiable in the Hipparcos database for stars with parallax error less than ten percent.

Then, by analysing the Hipparcos clump and model generated clumps, they assert that the bluest extreme of the red clump contains younger more massive fainter stars in comparison to the other clump stars. This blue extreme of the clump contributes to the mean clump magnitude estimate because its separation from the main red clump is not distinct. The actual weight of this affect is stated to be dependent on two factors:

- The relative proportion of young stars (about 1 Gyr old) to older stars.

- The definition of the colour interval used to measure mean clump magnitude M_I.

This is used to explain how the Magellanic Clouds, with a lower mean metallicity, are observed at bluer colours and partially exceeds the interval that the Hipparcos clump specifies. Thus the sampling of clump stars must be done with keen attention to these systematic errors that may arise

in the measurement of M_I. Even though M_I may be constant over the clump, it still shows a metallicity dependence, i.e. for a galaxy with a lower mean metallicity value M_I will be systematically brighter.

It is believed that the reason that the distance calculated to the Galactic Centre by P&S was not affected by systematic errors is because populations with metallicities varying between solar and twice that amount, the increase in clump mean magnitude may be reversed if helium content increases proportionally to Z. This is also mentioned by Cole (1998), asserting that "in real stars, Y increases with Z, and core mass Mc decreases with increasing Y (Sweigart and Gross, 1978)" They conclude that if distance determination is made where M_I is assumed to be independent of the stellar population, then that distance would only be accurate to 0.5 mag, which is too large for reasonable distance measurements. It seems that an empirical study into the helium content of the red giant stars or the red clump stars in the Bulge may be worthwhile in light of the effect that helium may have on the red clump mean magnitude. However, such a study is beyond the scope of this project due to time limitations.

2.3.3 Empirical Investigations

At this stage it was fortunate that the desired empirical tests of model predictions became available. A comprehensive investigation was made by Udalski (1998a) into the stability of M_I with respect to metallicity whereby the RR Lyrae mean V-band luminosity at the metallicity of the Galactic Bulge region was used as a reference brightness to analyse M_I in objects of different ages and metallicities. Huge samples of field RR Lyraes were used including 73 from the Galactic Bulge, 110 from the LMC and 128 from the SMC. The RR Lyrae distance scale was calibrated with the recent calibration of Gould and Popowski (1998) which was based on statistical parallaxes. Udalski found a weak M_I dependence on metallicity and its zero point was calibrated using Hipparcos red clump stars resulting in the equation used for calibration :

2.5 $$M_I^{RC} = (0.09 \pm 0.03) \times [\frac{Fe}{H}]^{RC} - 0.23 \pm 0.03.$$

The revised clump distances to the bulge, LMC and SMC were in good agreement with the RR Lyrae distances supporting the short distance scale idea that he formerly expounded.

The relationship between the V-band absolute magnitude and metallicity was taken to be

2.6 $$M_V^{RR} = (0.18 \pm 0.03) \times [Fe/H]^{RR} + const$$

and was derived based on observations of RR Lyrae stars from the Galaxy. It was assumed that the same relation would hold in other galaxies. The mean [Fe/H] of RR Lyrae stars in the bulge has been well determined in a spectroscopic survey by Walker and Terndrup (1991) to be $[Fe/H]^{RR} = -1.0$ with a dispersion of 0.16. The metallicities adopted for the LMC and SMC RR Lyrae stars were -1.6±0.2 and -1.7±0.2 respectively. The absolute calibration of the RR Lyraes was based on statistical parallaxes of about 150 stars derived from ground based and Hipparcos proper motions (Gould and Popowski, 1998). The mean absolute luminosity using a metallicity of -1.0 and a 0.18mag/dex relationship for metallicity was found to be

2.7 $$M_V^{RR} = 0.88 \pm 0.14 mag$$

The distance moduli were obtained by finding the difference between the V band brightness calibrated for Bulge metallicity and the mean absolute magnitude written above.

Thereafter, a straight line is graphed for the difference between the mean I-band brightness of the clump stars and the mean V-band luminosity of the RR Lyraes reduced to Bulge metallicity, against the metallicities of the clump in the LMC, SMC, GB and the Carina galaxy. A trend is observed between mean red clump magnitude and metallicity of an object. Hipparcos stars are then

used to calibrate the zero point of the brightness-metallicity relation for the red clump stars resulting in the equation for M_I^{RC} formerly mentioned.

A further empirical test was conducted by Udalski (1998b) and displayed the constancy of M_I^{RC} with respect to age in the range of ages from 2-10 Gyr. Fifteen star clusters of age varying from 1.5 to 12 Gyr were observed in the haloes of the LMC and SMC and their subsequent values of M_I were calculated for mean metallicities of -0.8 for the LMC and -1.2 for the SMC. They noted that for objects older than 10 Gyr, the mean clump magnitude could be up to 0.3 to 0.4 magnitudes fainter, thus setting a limit on the clump distance technique. The obtained clump magnitudes were in good agreement with each other and previous determinations, being; 17.88 mag for the LMC with a standard deviation of only 0.05 mag and 18.31 mag for the SMC with a standard deviation of 0.07 mag. The main contributors to the errors occurred where the clump was poorly defined and where the geometrical correction was uncertain. It seems that the red clump technique of measuring distances has at this stage been carefully empirically analysed and calibrated such that it can be trusted as a secondary distance indicator. Indeed, even a recent calculation of the distance to M31 (Stanek and Garnavich,1998) using the red clump stars has yielded a distance of R=784±13±17kpc in good agreement with a recent determination of Holland (1998) which uses the red giant branches of globular clusters occurring in M31.

CHAPTER THREE: Data Reduction and Error Analysis

3.1 Introduction

The data was collected as a by-product of the PLANET (Probing Lensing Anomalies Network) microlensing survey. This is a coordinated campaign to monitor microlensing events continuously with telescopes distributed at large intervals of longitude in the southern hemisphere. The Cousins I-band and the Johnson V-band are monitored in order to obtain precise photometry with minimal exposure time in all phases of the moon. In 1997 the survey included the SAAO 1m telescope at Sutherland in South Africa, the Canopus 1m telescope in Hobart, Tasmania and the Dutch 0.91m telescope at the European Southern Observatory on La Silla.

All data presented here were imaged on the SAAO 1m telescope. This is located at longitude and latitude of 20.81 and -32.8 degrees, has a pixel scale of 0.35" and a CCD format of 512X512 pixels. Images were flatfielded and debiased using mean flats measured at twilight. The on-line reduction at SAAO is performed by the DoPhot package. A catalogue of positions was established for objects in each field, using the best quality image of that particular field, and ten stars were chosen as reference stars which were used to monitor the progress of an event through varying weather conditions, and served as a guide to reduction difficulties which may result from poor seeing conditions, CCD guiding errors or transparency fluctuations. The flux of the microlensed source was expressed as a fraction of the average flux of the reference stars, which would later be calibrated using photometric standard stars.

The exposure time for each field was typically about 5 minutes in I and about 10 minutes in V. The official names of the fields are written in the form MACHO 97-BLG-31 etc. but PLANET uses shortened names (e.g. MB9731) for convenience. Further information about the PLANET microlensing campaign may be found in Albrow et al (1999).

3.2 Setting the Zero Point

In order to obtain astronomically useful information, we need to have photometry on a standard system. This involves setting the zero point for each field and correcting the observed magnitudes for colour equations. A catalogue of E-region standard stars was used to set the zero point for the observed fields (Menzies et al, 1989). The magnitudes and colours for the E-region standard stars have been determined to a precision of a few thousandths of a magnitude.

In order to ensure that photometric conditions were stable over a night, the observations of program stars were bracketed with observations of about eight to ten E-region standards. The instrumental magnitudes are recorded by an aperture measurement centred on the star in which the total number of counts per second received is recorded. The sky background is estimated from an annulus outside the star aperture. DoPhot does this automatically and subtracts the background sky measurement from the initial measurement yielding a corrected instrumental magnitude. The instrumental magnitude can be described by the equation

3.0 $$i = -2.5\log(counts/\sec)$$

Having the magnitudes I of the various E-region stars, enables us to make a comparison with the instrumental magnitudes i of the E-region stars, so as to find the zero point of calibration of our instrument to standard magnitudes. This is done by making a plot of the difference between the instrumental magnitudes i, v and known magnitudes of each E-region star $(i-I)$, $(v-V)$ against the known $(V-I)$ value for each star. A straight line is plotted through the points, yielding a zero point value and the slopes a and b associated with the equations:

3.1 $$i - I - k_I \sec z = a(V-I) + Z_I ,$$

3.2 $v - V - k_V \sec z = b(V - I) + Z_V$,

where $k \sec z$ is the correction for extinction and k is the absorption coefficient of the earths atmosphere.

The slopes for each wavelength band on each night are found by fitting the equations above. The slope is dependent upon instrumental factors such as the reflectivity of the mirror, the filters used and the CCD detector. Since these factors are expected to be more or less constant from night to night, the slope variation between nights can be regarded to reflect whether the nights were photometric or not.

Certain anomalous observations of standard stars were selected for omission. If stars exhibited behaviour that implied variability they were omitted. In addition, a check was employed to ensure that the proximity of one E-region star to another was not close enough to impair the recorded measurement. This was done using the catalogue of E-region stars (Menzies et al, 1989). It should be stressed that great care was taken to avoid influencing zero point compatibility between nights by omitting stars for no reason.

Where good agreement between the slopes between different nights is found, a mean slope may be adopted for a subsequent fitting of equations 3.1 and 3.2, which would then yield zero point measurements for each night. Thereafter, the deviation of each point from the line drawn with the mean slope will be determined, and its variation in time established.

Results:

It was found that the slopes a and b in the equations above, were in close agreement for two nights of observation. Discrepant values obtained for an intervening night suggest that conditions were not photometric then. These shall henceforth be referred to as night one and night two respectively. The slopes associated with the I filter for night one and night two were -0.066 and -0.075, while the slopes associated with the V filter for nights one and two were -0.048 and -0.025

respectively. The deviations of each point from the line in each case were lower than that of the following step, as they should be. This may be seen below.

Table 2.These are the tabulated results. These tables exhibit the straight-line plots for night one and two in I and V, and their associated slopes, intercepts and standard deviations. The figures below show the corresponding linear fits to the data.

I	Night One	Night Two
a	-0.066	-0.075
Intercept (mag)	-21.147	-21.145
No. of Stars	30	27
Standard Deviation	0.016	0.021
----------	----------	----------
V	Night One	Night Two
b	-0.048	-0.025
Intercept (mag)	-21.697	-21.697
No of stars	28	21
Standard Deviation	0.019	0.01

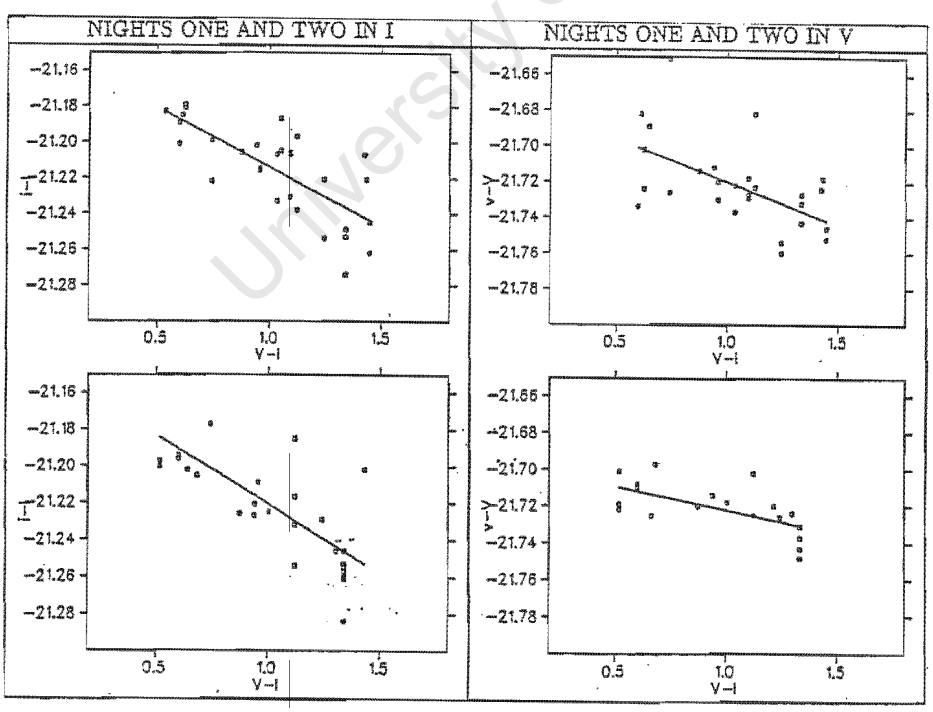

Figure 1: These figure exhibit the straight line plots made using the adopted mean slopes.

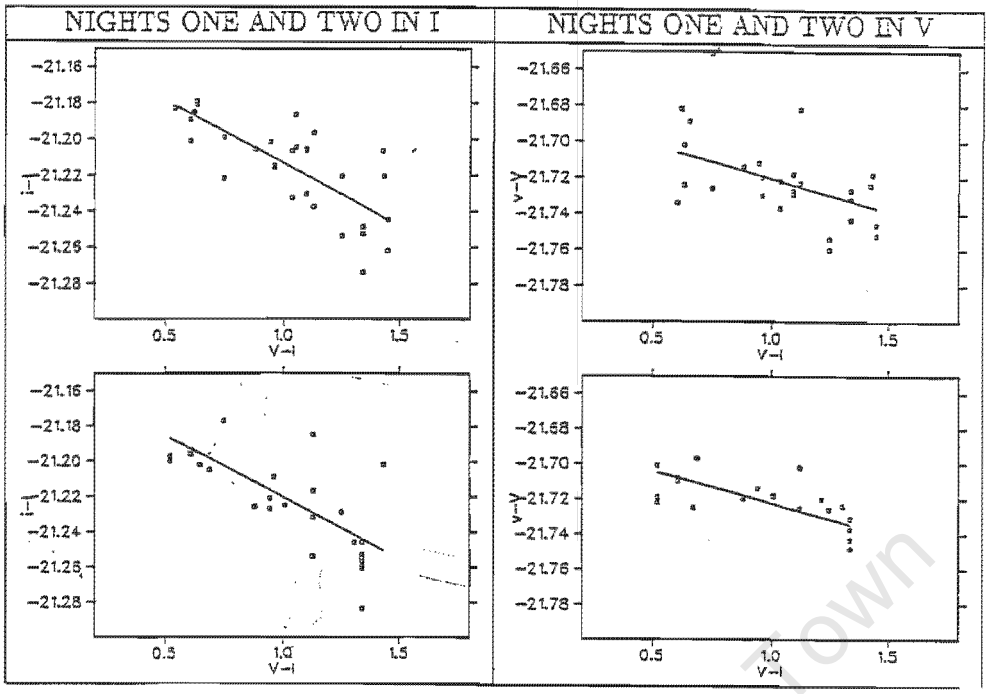

In all the figures exhibited in Table 2, the y-axis corresponds to the left hand side of the equations 3.1 and 3.2 while the x-axis corresponds to the $(V-I)$ term on the right hand side of these equations. The mean slopes adopted for the I and V filters were -0.070 and -0.036 respectively. Using these mean slopes, the calculated zero points in I for night one and night two were -21.144 and -21.151 respectively, while the zero points in V for night one and night two were -21.685 and -21.686 respectively. Figure 1 illustrates this.

The stability of the zero point was checked by indiscriminately leaving out stars after the reduction. The zero point did not vary from its adopted value outside that of the associated uncertainty, which is described in the next section.

Zero Point Variation With Time:

For each night, the deviation of each point from the line was calculated. In each case, most of the deviations from the line were within 0.02 mag, while the furthest points were at most 0.06 magnitudes away from the line. Zero point settings determined in other surveys of this kind usually have an error of about 0.05 magnitudes associated with it, however, but these usually are better constrained due to standard stars being recorded at higher photometric precision. While the

zero point does vary in time, the slope of the lines describing this variation is small. Night one exhibits the largest slope, and at the beginning of the night the deviation is -0.011 mag while at the end of the night the deviation is +0.013 mag. The results are presented in Figure 2 and Table 3.

Figure 2: This figure depicts the zero point variation with time for nights one and two while the results are presented in Table 3 below.

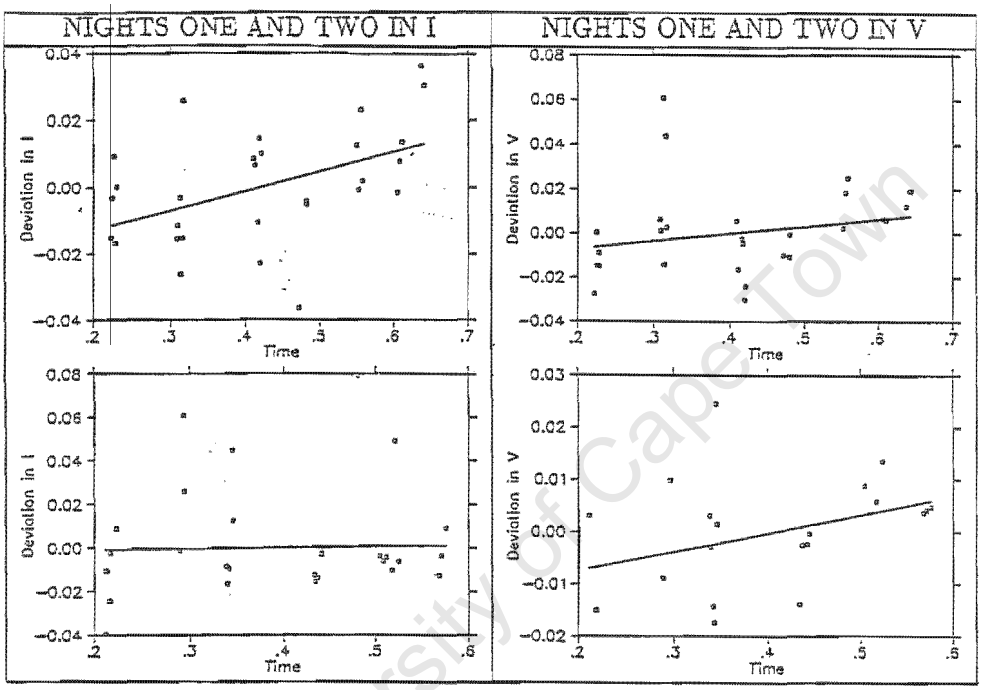

Table 3: These are the results corresponding to the figures above.

I	Night One	Night Two
Slope(units:mag per Julian day fraction)	-0.058	0.005
Intercept(mag)	-0.024	-0.001
Standard Deviation	0.016	0.015
V	Night One	Night Two
Slope(units:mag per Julian day fraction)	0.034	0.035
Intercept(mag)	-0.014	-0.014
Standard Deviation	0.020	0.021

We can now make use of the relation between deviation and time to derive the equations that would describe how the zero point varies in time. Using 3.1 and 3.2 we can see that where the deviation in time may be expressed as;

3.3(a) $deviation = m(time) + c$,

3.3(b) $Z_I(t) = i - I - k\sec z - a(V - I) - m(time) - c$, and

3.3(c) $Z_V(t) = v - V - k\sec z - b(V - I) - m(time) - c$.

These equations describe how the zero point would change in time. This relation will be needed when the measurements of fields at different times during the night are being reduced.

3.2.1 Reduction of Frames

The recorded frames were 3×3 arcmin in dimension. The reduction of each field and the matching up of stars in different frames were all done by the DoPhot package. In the reduction of each frame an aperture magnitude and the peak of the fit of a Gaussian profile was recorded:

3.4 Aperture magnitude = -2.5log(Aperture Counts)+27

3.5 Fit magnitude = -2.5log(Peak Counts)+27

The arbitrary constant 27 was added in order to make the magnitudes positive for convenience.

It has been described how the aperture measurements of E-region standard stars were corrected for the effect of the sky background. For the frames taken of the observed fields, however, the same method cannot be used because the fields are considerably crowded. In order to provide true aperture measurements of stars in the frames that may be corrected

with the zero point derived from the sky background corrected E-region standards, we had to employ the process which shall be described shortly.

Figure 3: This is an example of how the difference between fit magnitudes and aperture magnitudes may be seen to stabilize at brighter magnitudes while at fainter magnitudes the difference varies more.

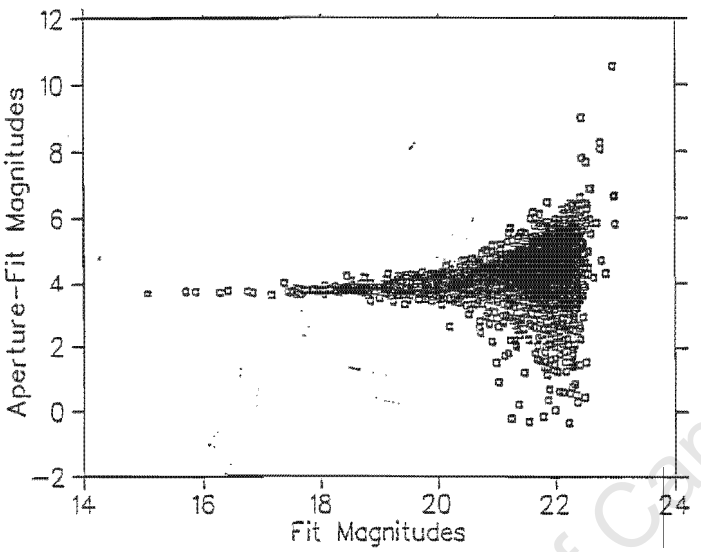

Now, while the aperture magnitudes are relatively invariant, the fit magnitudes no doubt vary with factors like seeing. Bad seeing would mean the Gaussian fit is more spread out or is flattened, and a correlated drop in peak magnitude can be expected. To compensate for this the average variation of fit magnitudes from aperture magnitudes must be quantified. Plotting the difference between fit and aperture magnitudes against fit magnitude shows a more stable distribution at brighter magnitudes (as expected). For each frame a plot of this was made (see Figure 3).

Thereafter the more stable section was subdivided into one magnitude ranges for which an average value was calculated and in addition, a histogram of the number of stars N_s versus $Fit - Aperture$ magnitudes was fitted with a Gaussian profile and the average fitted

$Fit - Aperture$ recorded. The values generally agreed well, and where the ranges seemed to stabilize a value was chosen, i.e Z_I' and Z_V'.

It was then possible to calculate the effective aperture $Apefftrue$ simply using;

3.6(a) $$Apefftrue(I) = FitI - Z_I' - 27 + 2.5\log(INTEGRATION\_TIME)$$, and

3.6(b) $$Apefftrue(V) = FitV - Z_V' - 27 + 2.5\log(INTEGRATION\_TIME).$$

Atmospheric effects were then corrected for using the standard values for k_I and k_V coefficients used at Sutherland. These values were compared with those determined with the 0.5m telescope on the same nights and were not found to be significantly different. In addition, the zero point was corrected for yielding the required corrected apparent magnitudes I_{app} and V_{app}.

3.7 $$I_{app} = FitI - Z_I' - 27 - 0.07\sec z - Z_I(t) + 2.5\log(INTEGRATION\_TIME)$$

3.8

$$V_{app} = FitV - Z_V' - 27 - 0.15\sec z - Z_V(t) + 2.5\log(INTEGRATION\_TIME)$$

3.9 $$k_I = 0.07$$

3.10 $$k_V = 0.15$$

The equations below,

3.12(a):

$$I_{app} = FitI - Z_I' - 27 - 0.07\sec z - Z_I(t) + 2.5\log(INTEGRATION\_TIME)$$

3.12(b):

$$V_{app} = FitV - Z_V' - 27 - 0.15\sec z - Z_V(t) + 2.5\log(INTEGRATION\_TIME)$$

summarise how the apparent magnitudes are arrived at.

Error Analysis

Considering equations 3.1, 3.2, 3.7 and 3.8, we may derive the simple equations

3.14 $I = I_{app} - a(V - I)$

3.15 $V = V_{app} - b(V - I)$, where

3.16(a) $I_{app} = i - k_I \sec z - Z_I$

3.16(b) $V_{app} = v - k_V \sec z - Z_V$, and

where I and V represent the known values of E-region standard stars, and the mean slopes a and b are those which were determined earlier. I_{app} and V_{app} are the airmass and zero point corrected measurements that we have made of these same standard stars. An iterative process may be employed to analyse how the standard stars would behave if they were treated as program stars. We can let $(V - I)$ be some arbitrary value 0.5, and calculate I and V. We can then calculate $(V - I)$, which may be substituted for $(V - I)$ in the equations above and used to recalculate

I and V. This process can be iterated until convergence between I and V values are reached. These I and V values should be comparable to the I_{cat} and V_{cat} values appearing in the catalogue which have been determined to a precision of a few parts in a thousand.

The differences $(I - I_{cat})$ and $(V - V_{cat})$ would then reflect the true deviations in the value of the zero point. The standard deviations would be $(\sum(I - I_{ca})^2 / N)^{1/2}$ and $(\sum(V - V_{ca})^2 / N)^{1/2}$ (where N is the number of stars used in each case) and would reflect the standard deviation or the most probable error in the calibration of the program stars to the standard system using time variant zero points.

The results for this exercise yield standard deviations 0.016 and 0.023 in I for night one and night two, while yielding 0.021 and 0.014 in V for nights one and two respectively. These standard deviations are in agreement with what should occur based on standard deviations occurring in the data evaluated up to now. The standard errors associated with I are 0.03 and 0.05 for nights one and two respectively. In V, the standard errors are 0.004 and 0.003 for nights one and two respectively. These errors are representative of the samples of E-region standard stars used, and show consistency in the zero point determinations on different nights. When the zero point is applied to an entire field of stars, however, crowding in the field complicates the accuracy of measurement and it would be safer to regard that error associated with the zero point of the red clump stars as 0.02 (the Dophot formal error described below).

Then, each star in a given field is corrected for the colour equations in a process similar to that outlined above. The final I_f and V_f for each star in the field is found by iterating the equations

3.14(a) $I_f = I_{app} - a(V - I)$

3.15(a) $V_f = V_{app} - b(V - I)$

where $(V-I)$ is taken to be $(V_{app}-I_{app})$ at first and the equations are iterated using the same a and b values until convergence is reached between consecutive I_f and V_f values respectively.

3.3 Colour-Magnitude Diagrams

3.3.1 Error Analysis

DoPhot outputs the error in magnitude of each fitted star and an error analysis was done. A plot of magnitude error versus fit magnitude was made and was fitted with exponential limiting functions on both sides of the distribution. Stars observed at brighter magnitudes should have relatively small errors in comparison to those at fainter magnitudes. The exponential functions chosen to limit the errors reflect this expectation. If a star at bright magnitudes has a large error associated with it, then the measurement cannot be trusted, and no assurance can be given that the star is indeed part of the Bulge population. In addition, it ensures that the stars in each frame would be carefully chosen to be suited to the modified Gaussian fit that would be used to get the mean magnitude of the red clump. Even in the faintest magnitude regions (where the error is largest) no star with a DoPhot formal error more than 0.2 magnitudes was chosen. In the magnitude range that the red clump occurs, the DoPhot formal error is considerably less (less than 0.02 mag). An example of one such reduction is shown in Figure 4.

Figure 4: A typical reduction performed on a field of bulge stars. The exponential functions on either side of the distribution represent the cutoffs for selection of stars. Any stars above the upper exponential function or below the lower exponential function were omitted

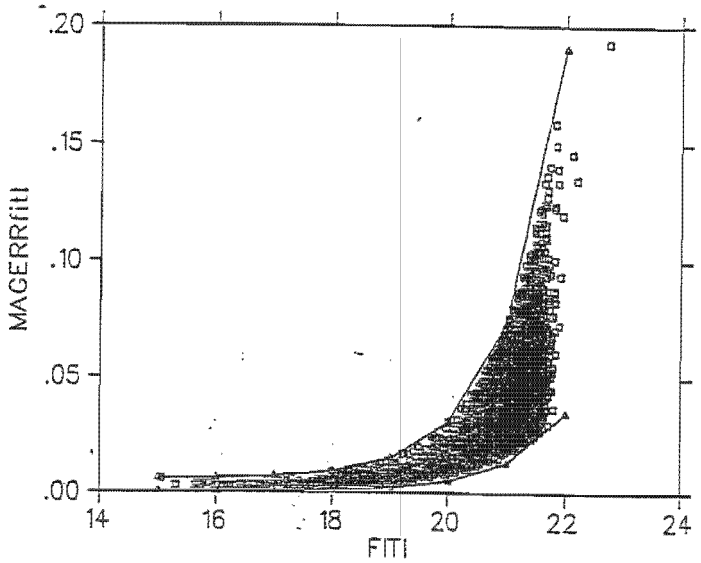

The very same kind of error reduction was performed on the V magnitudes.

Results:

The colour magnitude diagrams I versus $(V-I)$ were drawn using the equations 3.12(a) and 3.12(b), and after this whole process had been implemented for a particular field in the I and V magnitudes then the stars can be matched up in both frames using the Dophot star number label, and a colour magnitude diagram can be produced.

Comparison of different observations of the same fields reveal a consistent well calibrated data set that is suitable for distance measurement. The fields, when compared to extinction corrected fields of the Bulge (e.g. P&S), reveal that the fields are shifted by about two magnitudes fainter in V. It must be noted that the corrected fields were in Baade's window of low extinction where extinction has a minimum of about 1.5 magnitudes and a maximum of about two V magnitudes (Stanek, 1996). An example of one such field observed on nights one and two is shown in Figure 5.

Figure 5:These are observations of MB9750 on night one and MB9749 on night two. Less stars were observed on night two. Otherwise, their similarity is a good indication that the magnitudes were derived correctly in the aforementioned processes.

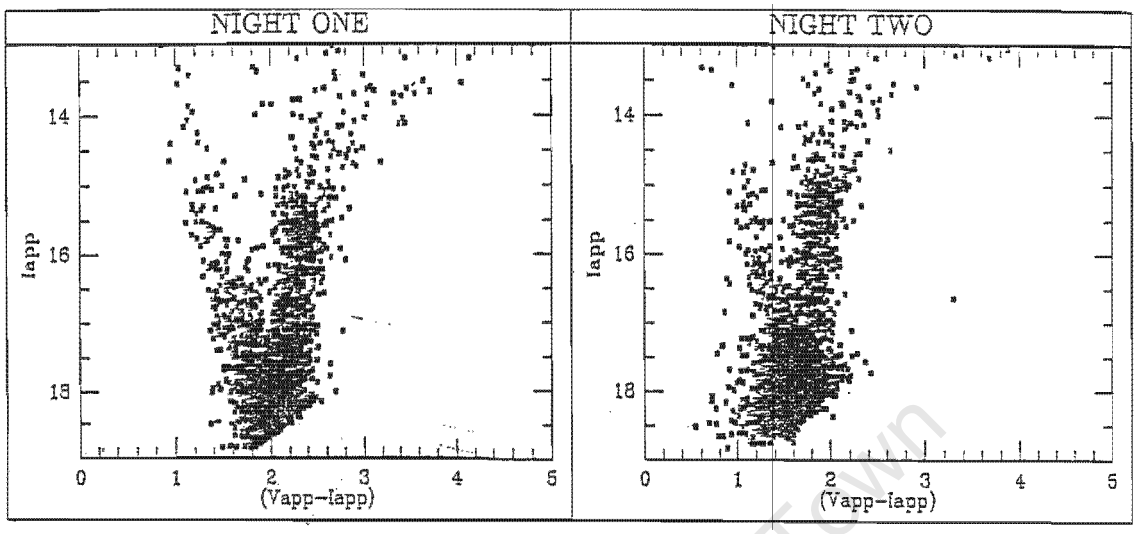

An instrumental cut-off is observed i.e. a diagonal cut-off running from about the 18th to 17th magnitude. This is not an evolutionary feature but arises because the V band limit is constant $(V_{\lim})$. Since $I = const - (V_{\lim} - I)$, an increase in $(V - I)$ by 1.0 leads to a decrease of I by 1.0. The red clump itself can clearly be seen on the red giant branch, which suffers from considerable crowding.

3.3.2 Reddening and Extinction

An all-sky reddening map was recently published using data from the COBE/DIRBE and IRAS/ISSA surveys by Schlegel, Finkbeiner and Davis, (1998, hereafter: SFD). The map, while being accurate at higher galactic latitudes, was regarded as inaccurate for latitudes within $|b| < 5°$.

However, recently, Stanek (1998) made an investigation into the reddening values of the SFD within this latitude range and found that it overestimates the reddening by a factor of about 1.36. This was established by using the reddening map of Baade's Window and a sample of 19 globular clusters for which the reddening is given by the catalog of Harris (1996). The reddening values

predicted by SFD were compared with the known values, and a straight-line relation was graphed between the two. This straight-line relation yielded a factor around 1.36. This may be written;

3.17(a) $E(B-V)_{SFD} = 1.36E(B-V)_{GC+BW} - 0.02$

In addition, the relation between the SFD map and the globular clusters alone was found to be

3.17(b) $E(B-V)_{SFD} = 1.50E(B-V)_{GC} - 0.26$

While these relations are useful in the region $|b| < 5^o$, it may be misleading in high reddening regions close to the Galactic plane $|b| < 2^o$. One of our fields, MB9741 was located too close to the Galactic plane for this reddening relation to be used. Both relations yield similar values if $E(B-V)$ is close to the value 1, however, for values deviating from 1 there is a significant difference between the values that the relations yield.

It was decided that the second relation (3.17(b)) provided a better account of the reddening in the region and this was the relation that was subsequently used. Although the I magnitudes were similar for both relations, it seems that extinction in V was underestimated by 3.17(a) yielding a clump that seemed shifted too far to the red on the $(V-I)$ axis. Since Baade's Window is a region of low reddening it was felt that using a large number of points from it might result in the relation 3.17(a) being biased towards lower reddening values.

Each field is corrected for reddening in such a way that every star is individually corrected for reddening. The reddening across a field changes gradually, so an evenly spaced grid with high resolution will yield reddening values that are within small enough experimental error to be used. Reddening across the Galactic Bulge, however, may vary greatly due to the concentration of dust and filaments of dust that occur there. It is important to note that the microlensing surveys are focussed on windows of low reddening in the Bulge. This is due to the need to observe large numbers of stars in the hope of detecting a microlensing event. Thus, the observed fields can with

confidence be regarded as having a more or less uniform distribution in reddening, with slight gradients occurring in some cases across the field. The values of reddening $E(B-V)$ may change from values as low as 0.6 to values as high as 1.4 (in extreme cases of variation in reddening), but typically range between about 1 and 1.4.

A grid of values is obtained for each 3×3 arcmin field. The grid is then divided into 400 squares (i.e. spaced as 20×20) and a value of reddening is derived at each point. This indicates that the gradient would at the most 0.04 magnitudes per block (i.e. (1.4-0.6)/20, using a change of 0.6 to 1.4 from one side of the field to another) while for most of the fields it would more likely be about 0.02 (using a change of 1 to 1.4 from one side of the field to another). The standard deviations that could be expected would be 0.008 and 0.004 respectively. The unweighted statistical error associated with these values is 0.006. This value overestimates the error because it is unweighted but is sufficiently descriptive of the error and it is this error that we regard as the error associated with the reddening grid. This is, however, only an account of the statistical error in the measurement and makes no attempt to evaluate the systematic error that could result from the filamentary dust structure (SFD, 1998) occurring within the resolution adopted here.

After the grid is established and a reddening value allocated to each vertex in the grid, a program determines the reddening of each star using the coordinate location of the star. The grid consists of 400 'boxes' within which the stars in the field may be located. In any given box the reddening values will be located at the four vertices enclosing the box. If the star is located within a certain 'box' in the grid then it will be assigned the largest of the values of reddening located at its vertices. Reddening increases in value towards the Bulge (i.e. in the x direction), and therefore the chosen reddening value often corresponds to that of the vertex that is closer to the bulge. In this way, a value of reddening is attained for each individual star.

This $E(B-V)$ reddening value is then converted to $E(V-I)$ using the universal relation

3.18 $E(V-I)=1.3\times E(B-V)$.

The value 1.3 is the universal relation adopted by Stanek (1998). Thereafter, in order to get the visual extinction in magnitudes, the relation

3.19 $A_V = (2.49 \pm 0.02) \times E(V-I)$

which was determined for Baade's window (Stanek,1996), was used. The ratio 2.49±0.02 was deemed appropriate in light of the investigation into the selective extinction across the Bulge (Wozniak and Stanek, 1996). Although the ratio varied from 2.35 to 2.66 across latitudes zero to five of the Galactic Centre, all values agree within their associated errors and the value 2.49 can be used.

Wozniak and Stanek used the red clump stars of OGLE bulge fields lying between $-5° < l < 5°$ to construct the reddening curve and obtained results that were consistent with the constant value of the extinction to reddening ratio expressed in equation 3.19.

Then, subfields with different extinction are separated and used to construct a reddening curve. The method used to separate subfields is quantitative. For each field, a list of stars contained in this field was extracted with their V magnitude and position on the frame. Only stars with V≤20 mag were used in order to ensure completeness against field crowding. Each frame was divided into 32× 32 subframes and the total number of database stars in each frame (with V≤20) were computed, and were on average 15-100 in each subframe. The subframes are then arranged into 16 groups in order of increasing number of database stars per subframe, with each group containing roughly the same number of stars. The ordering of subframes should then reflect a decreasing extinction in a group. The shifts in reddening and extinction for each subfield are obtained and the random errors of these values are ascertained using a bootstrap technique.

Stanek (1996) applied the method of Wozniak and Stanek to map the interstellar extinction for the Baade's window region of the Galactic Bulge. The method is applied to star density maps of nine Baade's window fields in a roughly 40×40 arcmin region of Baade's window. A straight line is

fitted to the results and the relation 3.19 is obtained from the fit. This value is close to the value 2.6 obtained by Dean, Warren and Cousins (1978) and Walker (1985).

The extinction in I is calculated using

3.20 $A_I = A_V - E(V-I)$,

and finally, the extinction corrected values for the V and I bands are calculated to be

3.21 $I_c = I - A_I$, and,

3.22 $V_c = V - A_V$.

Foreground Stars

Now, one may expect that foreground stars along the line of sight which passes through the disk towards the Bulge, may be allocated wrong values of reddening by the SFD map, and may contaminate the red clump and thus affect the estimate of its mean magnitude. However, there are much fewer foreground stars occurring in a 3×3 arcmin field than Bulge red clump stars. Indeed, these would in some sense be dealt with by the additional terms in the fitting function 2.1 that is used to calculate the mean magnitude of the clump. In addition, the disk clump stars can barely be seen as an enhancement in the number of stars upwards of the Bulge red clump. The foreground stars make up about ten percent of the total number of stars at $V = 18$ but only two percent of the stars at $V = 20$ (Holtzman et al, 1993).

Results:

Following the procedure outlined above, the fields were corrected for extinction, and equations 1.21 and 1.22 were used to generate the colour magnitude diagrams. The same two fields that were presented in the preceding section now corrected for extinction are shown in Figure 6. The extinction corrected fields are all similar, with the clumps hovering around 14th magnitude. The red clumps are well populated, and thus may confidently be used for distance calculations. Table 4 contains the vital information used in reducing all the fields.

Figure 6: This table exhibits the extinction corrected colour magnitude diagrams for object MB9750 on night one and MB9749 on night two.

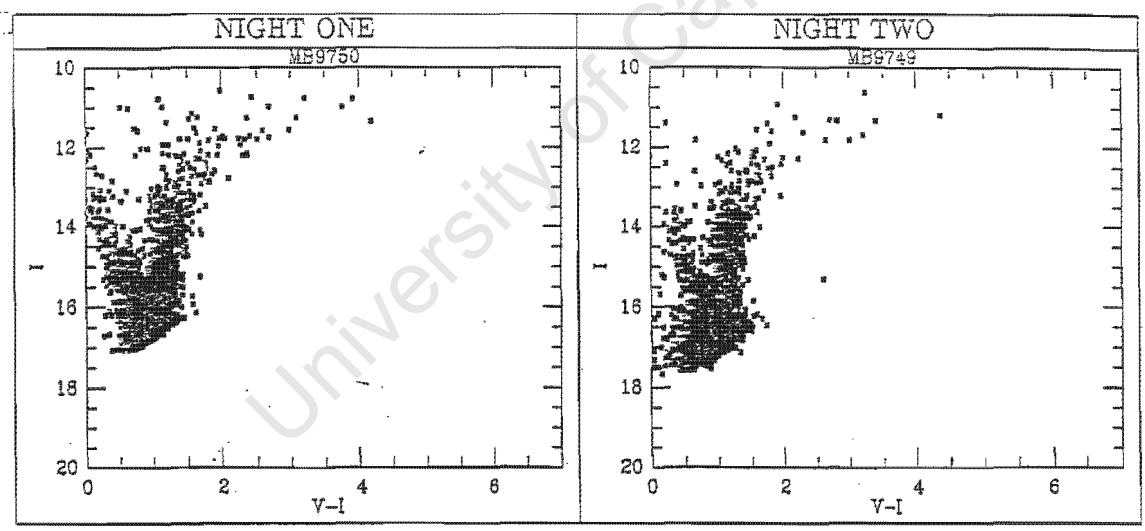

Table 4: The table shows the values for reddening at the centre of each field i.e. x and y coordinates (255,255).

	MB9726	MB9728	MB9731	MB9741	MB9749	MB9750	MB9731	MB9741
(l,b)	(1.026,-3.116)	(2.48,-2.40)	(5.116,-2.603)	(1.34,-1.98)	(1.92,-3.07)	1.977,-2.032)	(5.116,-2.603)	(1.34,-1.98)
$E(B-V)$	0.85	0.91	1.15	0.99	0.66	0.97	1.15	0.99
$E(V-I)$	1.105	1.183	1.495	1.287	0.858	1.261	1.495	1.287
A_V	2.75	2.94	3.72	3.204	2.136	3.13	3.72	3.204
A_I	1.64	1.76	2.227	1.91	1.27	1.878	2.227	1.91
Z'_I	2.91	3.67	3.71	2.68	3.65	2.85	2.65	3.62
Z'_V	2.75	3.85	3.80	2.83	3.80	2.80	2.63	3.62
I run no	3791143	3791479	3791463	3791139	3791444	3791141	3791187	3791477
V run no	3791144	3791480	3791464	3791140	3791445	3791142	3791188	3791478

CHAPTER FOUR: Results and Application

The method (P&S) utilised to calculate the mean magnitude of the red clump has already been described in chapter two. The defining characteristic of the fields on which this method has been used is that they contain many thousands of stars. Our fields do not. The reason is that our fields were considerably smaller in size (being 3×3 arcmin in dimension), and were not specifically chosen for this project. These fields are the by-product of the microlensing survey being conducted.

4.1 Modifications to Method

The standard procedure is to select clump stars within certain colour ranges and then bin the selected clump region into a histogram showing the number of stars in each magnitude range. This histogram is fitted with a function

$$4.1\ n(I_o) = a + b(I_o - I_{o,m}) + \frac{N_{RC}}{\sigma_{RC}\sqrt{2\pi}} \exp[-\frac{1}{2}(\frac{I_o - I_{o,m}}{\sigma_{RC}})^2]$$

in order to find the peak of this modified Gaussian function $I_{o,m}$.

As a consequence of the large number of stars observed in the large fields of the microlensing surveys, the intervals chosen to describe the red clump on the colour magnitude diagram could be chosen conservatively, especially on the V-I axis. The red clump falls comfortably into the interval $0.8<(V-I)<1.2$ mag for the Hipparcos stars (P&S), while for the Bulge fields, the clump falls in the interval $0.8<(V-I)<1.4$ mag. In order to fit the modified Gaussian function, stars consistent with the interval dictated by Hipparcos stars were chosen. Now while this may have been done in fields containing a large number of stars in order to preserve some kind of comparability between the Bulge and Hipparcos stars, the fact remains that the red clumps

occurring in the Galactic Bulge are already distinct in that their average $<(V-I)>$ value occurs at around 1.2 mag while the average $<(V-I)>$ value for Hipparcos stars occurs around 1.0 mag (P&S). Also, given that the reason for using this method in the first place is the constancy of the red clump mean magnitude over the entire red clump range (see P&S), there should be no significant reason why the entire $(V-I)$ interval of the Bulge fields should be used, and given the restricted number of stars occupying the Bulge fields in our survey, this is the approach we elected to use. If indeed, a trend with metallicity produces a gradient in the red clump mean magnitude, then we will have to be content with our use of the metallicity correction derived by Udalski (1998) mentioned in chapter two, viz,

4.2 $M_I^{RC} = (0.09 \pm 0.03) \times [Fe/H]^{RC} - 0.23 \pm 0.03$.

In order to use this metallicity calibration, the metallicity gradient found by Frogel (1999) within a few arc minutes of the Galactic Bulge was employed:

4.3 $[Fe/H] = (-0.064 \pm 0.012) \times b + 0.034 \pm 0.053$.

In effect, the final $I_{o,m}$ value will be that corrected for the effect of metallicity within the field, and thus its clump stars. While this relation is used, it may be useful to remember that the average [Fe/H] for this region is believed to be 0.0 (Frogel, 1999) which is in conflict with the values 0.29 and 0.44 established by high resolution abundance analysis of K giants in Baade's window (Whitford and Rich, 1983). This study suggests that the majority of their stars are super metal-rich. This however, does not constitute a result for the average metallicity of all the stars in the Bulge, indeed, the average metallicity for RR Lyrae stars in the Bulge was found to be -1.0 (Walker and Terndrup, 1991), while the average metallicity for M giants in the Bulge was found to be 0.3 (Terndrup et al, 1991), which is comparable to that of the K giants. It makes sense that the RR Lyraes exhibit a lower metallicity, being stars that occur on the horizontal branch, the metal poor equivalent of clump stars. To add to this an investigation into K and G giants using Washington photometry yielded an average metallicity of 0.17 (Geisler and Friel, 1992). It could be argued that

the average metallicities derived using K, M and G giants would better describe the metallicity of clump stars but a large range of metallicities is observed in these studies and ultimately, seeing that the clump metallicity correction relation (1.5) is rather weak, there is no reason why the relation derived by Frogel cannot be used.

The distance modulus m-M is still calculated using the absolute mean magnitude derived for the Hipparcos stars in P&S where M=-0.279±0.088, where the error is a very crude estimate of possible systematic error associated with their crude evaluation of extinction associated with the Hipparcos stars (P&S).

4.1.1 Statistical Error Evaluation

Firstly, the standard errors associated with the zero point have been established in the chapter on data reduction. These standard errors were very small. It was decided that the error in the zero point calcuation should be considered to be that of the formal DoPhot error 0.02 associated with the red clump stars. The statistical error associated with the grid would be about 0.006 mag at most. In addition, there is an error of 0.02 mag associated with the relation 3.19 used to calculate visual extinction. In order to calculate the error in the equation 3.19 an average $E(V-I)$ value of 1.2 was chosen so that the fractional error may be evaluated. This was found to be 0.01.

The errors associated with A_V and A_I are thus 0.01 and 0.011 respectively. The errors associated with I_c and V_c in equations 3.21 and 3.22 are thus 0.023 and 0.022 respectively.

In the fitting of the Gaussian peak, the standard deviation σ associated with $I_{o,m}$ has an associated standard error of $\frac{\sigma}{\sqrt{n}}$. The value of σ is usually quite small, the largest value being 0.17, and in general the standard error would be about 0.031 mag at most. Thus, the fitted mean magnitude $I_{o,m}$ has an error of 0.038 associated with it.

A further error of 0.04 mag is introduced into $I_{o,m}$ by making use of the metallicity calibration and the metallicity calculations according to equations 4.2 and 4.3. In order to calculate the fractional error associated with equation 4.3 we determine the values of [Fe/H] at the limits of galactic latitude 2<b<5. These limits indicate a range of 0.2 in the value of [Fe/H]. Putting this value into equation 4.2 then gives an uncertainty of 0.04 mag in M_I^{RC} (Udalski, 1998). This translates into a statistical error of 0.2kpc at most if this error is evaluated in the calculated distance to every field. This error is higher than that of other studies - about 0.4 kpc in the case of P&S but was corrected to 0.2 kpc by Stanek & Garnarvich (1998). It is important to note that a large part of the error is introduced by the use of the metallicity calibration, which implies that studies that make use of crude metallicity estimates may find that their errors are in fact larger. In addition more accurate metallicity studies may enable this distance calculation technique to be refined even further. In any event, it is encouraging nonetheless that a study such as this that uses red clumps that contain less stars by an order of magnitude than other studies still has a relatively small statistical error associated with it.

Now, the aforementioned crude estimate of systematic error in the extinction evaluation of Hipparcos stars carried out by P&S is 0.088 mag. If we include this systematic error in our consideration of our distance estimates the total error in the distance modulus would be 0.104. This translates into a maximum error of 0.4 kpc in our distance estimates.

4.2 Results:

4.2.1 The Colour-Magnitude Diagrams

Figure 7: The reddening corrected colour-magnitude diagrams for the analysed fields are presented here.

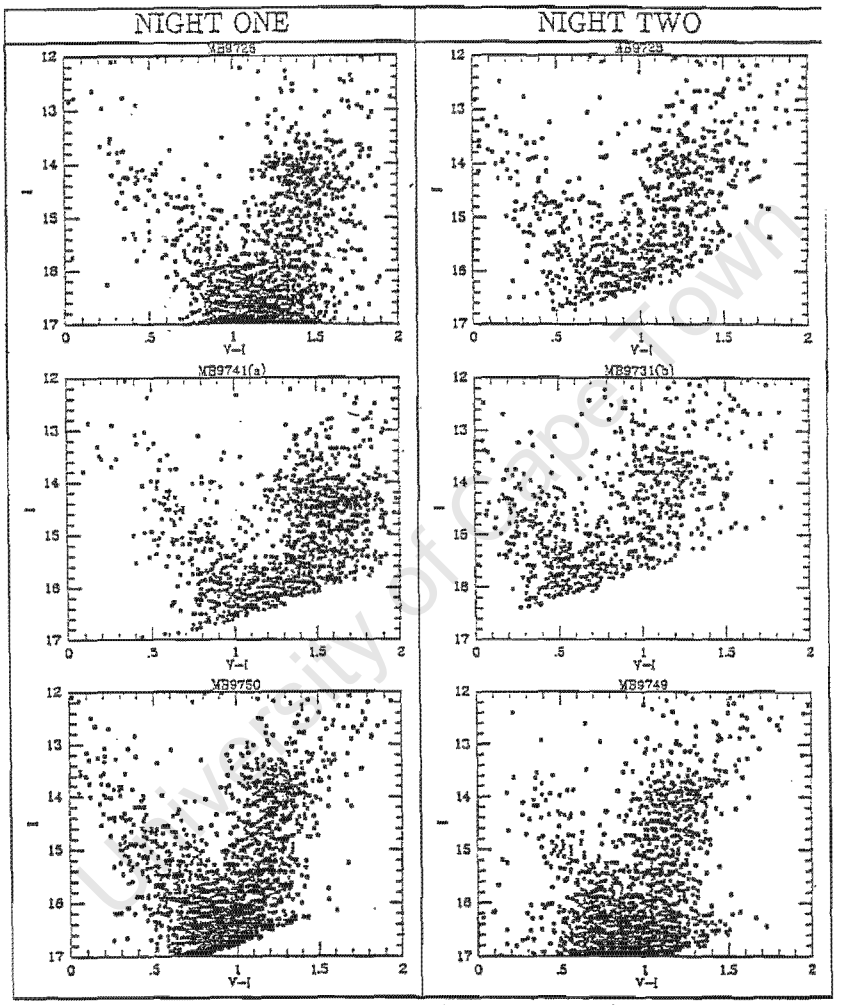

Shown in Figure 7 are the reddening corrected colour-magnitude diagrams displaying the observed red clumps. The red clump structures of MB9726 and MB9741 are clearly more reddened than the rest of the fields. The reason that MB9741 appears to be too red is that the relation used to correct for extinction is not valid for this field, being located in the region of galactic latitude $b < 2^{\circ}$

where the extinction correction equations are not valid (as mentioned in section 3.3.2). MB9726 is also shifted into the red and this may be because the SFD reddening map used may not have a fine enough resolution to fully reveal the variations in reddening in the region where it is located. In addition, it is close to the Galactic Centre in both galactic longitude and latitude and this may explain the excessive reddening that this field seems to exhibit. As it is, the map indicates patchy bits of reddening and drastic changes in reddening values across the field. MB9749 is located in the most suitable region for reddening to be established correctly. In any event, MB9741 and MB9726 are not used further in the investigation seeing that the reddening cannot be reliably determined for them.

4.2.2 The Red Clump Mean Magnitudes

The red clump mean magnitudes were found by fitting all stars in the intervals $13 < I < 15$ and $0.8 < (V - I) < 1.5$ with the modified Gaussian function. The intervals were chosen to include the maximum number of stars. The stars were binned and fitted by the Physica fitting package that uses a chi-squared reduction analysis to provide a fit. By selecting different sizes of magnitude bins and fitting the data with a chi-squared reduction analysis the sensitivity to different binning choices could be ascertained. The reduced chi-squared values indicate a poor fit to the data (values of 3 and above). This would be to our detriment if we were interested in the area under the curve, but it was found that the peak value stayed within our experimental error regardless of how large or how small the reduced chi-squared value was (and correspondingly, the different binning choices). It was therefore concluded that the reduced chi-squared value did not reflect the accuracy of the Gaussian peak i.e. the mean magnitude of the red clump. Indeed, it is a shortage of red clump stars that is responsible for the poor fit to the data. Featured in Figure 8 is a series of figures showing the modified Gaussian fit to the data.

Figure 8: This shows the modified Gaussian fit that was generated for the red clump of each

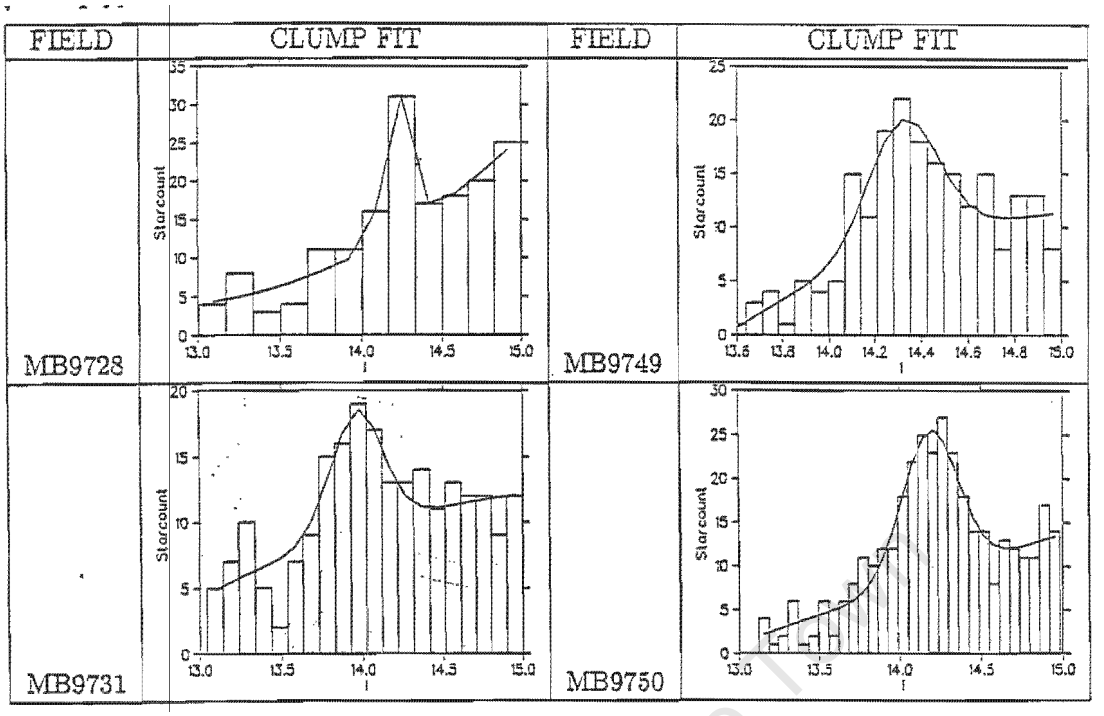

Table 5: The relevant individual field characteristics and the results of the fitting process are presented below. The final distance estimates are presented here.

	MB9728	MB9731	MB9749	MB9750
No of Field Stars	864	860	2503	2656
No of Clump Stars	245	221	208	353
$I_{o,m}$	14.22	13.97	14.32	14.19
σ	0.08	0.16	0.15	0.17
[Fe/H]	-0.12	-0.13	-0.16	-0.09
M_I^{RC}	-0.24	-0.24	-0.24	-0.24
$I_{o,m}(reduced)$	13.98	13.73	14.08	13.95
m-M	14.25	14.00	14.35	14.22
Distance (kpc)	7.1±0.4	6.3±0.3	7.4±0.4	7.0±0.4

Table 5 illustrates the results. The distance to the Baade's window field investigated by P&S is 7.65 kpc. The statistical error associated with the distances above is 0.2 kpc while the total error is 0.4kpc. That puts our distances in agreement with P&S within the associated error. MB9731 is the

only exception to that and given its location, may be located closer due to being part of the Galactic Bar structure.

4.2.3 Implications for the Galactic Bar Structure

In general, the distances are indicative of a Bar structure. In order to test the accuracy of the distances calculated above, it is worthwhile to include a rough study of how well their distances place them within the Galactic Bar. There are many ways in which the structure of the Galactic Bulge can be modelled. One may choose between Gaussian or Exponential type functions describing the volume emissivity of sources along the line of sight (see Dwek et al, 1995 or Stanek et al, 1997). Generally, each model is tested until a 'best-fit' to the data at hand is found. An investigation into the Bar using red clump giants was conducted and it was found that the E2 Bar model provided a best fit to the data (Stanek et al, 1997). They found that the inclination of the Bar to the line of sight lay between 20 and 30 degrees. This was in agreement with Dwek et al (1995) who investigated the variation of luminosity across the Bulge at different wavelengths in the near-infrared.

This inclination is best understood by viewing the Bar model in the x-y plane. In this plane, x increases in the direction of decreasing galactic longitude, while the z-axis is in the direction of increasing galactic latitude. The y-axis increases away from the observer. In order to relate the coordinates (x,y,z) to the line of sight distance s, we have equations:

4.2.1 $x = -s\cos(b)\sin(l)$

4.2.2 $y = -D + s\cos(b)\cos(l)$

4.2.3 $z = +s\sin(b)$,

where D is the distance to the Galactic Centre. This was chosen to be 8 kpc as this was the value chosen by Stanek et al (1997), and it is their model with which the comparison will be made.

In the investigation using the red clump giants (Stanek et al, 1997) figure 6 shows the resulting E2 model at 700 pc below the Galactic plane. In order to test the distances derived above it was a simple matter to generate (x,y) values and plot them onto the (x,y) axis so that comparison can be made with figure generated by Stanek et al (1997). Table 6 shows the results of this exercise.

Table 6: The location of the observed bulge fields according to the E2 Galactic Bar model (Stanek et al, 1997).

Field	x(kpc)	Y(kpc)	z(kpc)
MB9728	-0.31±0.02	-0.92±0.4	-0.29±0.04
MB9731	-0.56±0.02	-1.72±0.3	-0.28±0.02
MB9749	-0.25±0.06	-0.58±0.4	-0.39±0.04
MB9750	-0.25±0.04	-1.00±0.4	-0.27±0.04

The uncertainties associated with y are large because of the large uncertainty associated with our distances s. Plotted in Figure 9 are the fields projected onto the (x,y) plane. Their largest errorbars occur in y. Even with these large errors, the fields can clearly be seen to be contained within the limits predicted by the E2 Bar model by Stanek et al (1997), as seen in *their* figure number 6.

In addition, if a line is plotted through these points a gradient of 3.077 is found when the line is forced to pass through (0,0), while if the intercept is allowed to be variable, then a gradient of 2.99 is derived along with an intercept of -0.032. This may be loosely translated as implying an inclination of the bar at 19^{o}. Given that the uncertainties associated with each point are considerable enough to allow a large range of possible angles it is encouraging none the less that the fields are within agreement of the results shown in Stanek et al. Indeed, it is encouraging in the sense that the distances calculated show agreement with other studies. It is also an indication that if the distance to each field were to be corrected for its position in the Bar, and the distance to the centre of the Galaxy inferred, then that result would agree with that of P&S within experimental uncertainty. Seeing that the intercept generated was -0.032, this implies that my fields indicate an R_o distance of about 7.969±0.8 kpc which is consistent with the corrected distance

8.2±0.3 kpc of P&S.

Figure 9: The galactocentric distance is estimated using the E2 bar model of Stanek et al (1997)

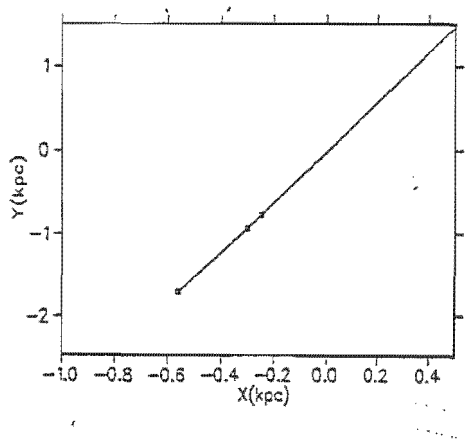

CHAPTER FIVE: Investigating the Microlensing Events

5.0 Introduction

This thesis has primarily been concerned with red clump stars in the observed fields. Data was obtained during the microlensing follow up campaign of 1997. Although limited data is available, I attempt to use it here to determine some properties of the microlenses. This approach cannot be regarded as definitive, but simply indicates what might be done in a case where more complete data is available for analysis.

5.1 Source Stars

5.1.0 Introduction

There are several ways in which the zero-point calibrated fields may be exploited for the analysis of their contained microlensing events. Firstly, it enables us to calibrate the light curve traced by the event, and secondly to make some kind of suggestion as to the spectral type of the source star being lensed. Thus, the mass of the source object may be inferred to some degree of accuracy. The light curve of a microlensing event involving a point source and a point lens is expected to be achromatic. It is thus expected to be constant on the $V-I$ axis of a colour magnitude diagram. Any deviation from this achromaticity would reflect the presence of an unresolved, unlensed star whose relative contribution to the observed brightness changes as the amplification varies through the event.

5.1.1 Photometric Calibration

The archived data included a lensing candidate and a number of reference stars surrounding the candidate. By comparing the reference stars to the stars in the observed standard star fields the difference between the two could be estimated and the reference stars recalibrated along with the light curve of the event. Only the fields MB9728, MB9731, MB9749 and MB9750 were evaluated

(the reasons for the selection of these fields has already been dealt with). The procedure may be broken down into a few steps:

- The i and v magnitudes of the reference stars from the archive were compared to those of the zero point corrected fields for which the procedure where the colour equations are taken into account had not yet been performed. When their differences are evaluated, the magnitudes show mean differences Δv and Δi between the two fields. The standard deviations from these mean differences $\sigma_{\Delta i}$ and $\sigma_{\Delta v}$ are also obtained.

- The i and v magnitudes of the reference stars are then corrected by adding the factors Δv and Δi to i and v where-after the colour equations are taken into account by the iterative procedure described in the previous chapter. The colour corrected I_c and V_c magnitudes are then compared to the original i and v magnitudes of the reference stars and the mean differences ΔV_c and ΔI_c along with their standard deviations $\sigma_{\Delta I_c}$ and $\sigma_{\Delta V_c}$ are again calculated.

- It was then that the archived i and v values for the microlensing light curves were corrected by the mean differences ΔV_c and ΔI_c. In order to find the average $(V-I)$, the light curves of the corrected I and V magnitudes were compared and could easily be judged by eye.

- Of course, extinction would then have to be taken into account and the extinction at the centre of each field noted in Table 4 was used, as this should coincide with the position of the lensing event. The final extinction-corrected mean $(V-I)$ values are presented in Table 7 as $(V-I)_f$. These are the values that will be used to determine the spectral type of the microlensing source stars.

Table 7: This table provides an account of the values calculated in the aforementioned four steps employed to reduce the data.

	MB9728	MB9731	MB9749	MB9750
$\Delta v \pm \sigma_{\Delta v}$	+0.09±0.06	0.58±0.07	-1.44±0.187	-0.3±0.07
$\Delta i \pm \sigma_{\Delta i}$	-0.11±0.06	-1.75±0.04	-1.73±0.176	-2.39±0.08
$\Delta V_c \pm \sigma_{\Delta V_c}$	+0.03±0.01	+0.52±0.02	-1.48±0.04	-0.39±0.01
$\Delta I_c \pm \sigma_{\Delta I_c}$	-0.28±0.03	-1.93±0.04	-1.85±0.13	-2.51±0.02
$(V-I)$	+2.6±0.04	2.91±0.06	1.7±0.306	2.15±0.10
A_I	1.78±0.04	2.26±0.04	1.28±0.04	1.87±0.04
A_V	2.99±0.03	3.78±0.03	2.13±0.03	3.13±0.03
$(V-I)_f$	1.39±0.11	1.39±0.13	0.85±0.37	0.90±0.17

The light curve of the lensing event can then be represented on an $I, V-I$ colour-magnitude diagram. From the location of the faintest end of the event i.e. when the source is at its baseline magnitude, one may decide whether the source star belongs to the main sequence or giant branch and the spectral index tables containing classification and in addition physical information about the types of star may be consulted. If the baseline magnitude is not available then one is unable to unambiguously determine the luminosity class of the source star. Thus, one should be able to estimate the radius of the source star involved in the event if one is confident of the baseline magnitude.

5.1.2 Spectral Types and Derived Parameters

The representations of the light curve of the lensing event depicted in both the $(I, V-I)$ colour magnitude diagrams and the $(V, V-I)$ colour magnitude diagrams are shown in Figure 10 so that the location of the faint end of the ordinate values might be compared, and a decision made as to which evolutionary structure the source star is indeed a part of; i.e. whether it is more likely located on the main sequence, the red giant branch, or may be best classified as a supergiant.

The faint end of the ordinate values are actually the faintest measurements of the light curve where it seemed indicative of the baseline magnitude to within a few tenths of a magnitude. So, in some sense we are dealing with a crude upper limit of the baseline of the microlensing curve and thus an upper limit on the source spectral type and the associated physical properties. However, similar studies conducted using the full microlensing light curve should give a more accurate illustration of possible source types. The source stars in fields MB9728 and MB9731 are more likely to be red giant branch stars whereas it is difficult to ascertain whether fields MB9749 and MB9750 are in fact part of the main sequence or the red giant branch, but seem more likely to be part of the red giant branch than the main sequence. It is also known that MB9728 is a binary lensing event, and a study of it has been made (Albrow et al, 1999). This will be dealt with separately, using the equations suggested by Albrow et al (1999).

Figure 10: These figures represent the light curve amplification on the colour-magnitude diagram of each field. The faintest end of the light curve represents the baseline of the light curve associated with the field.

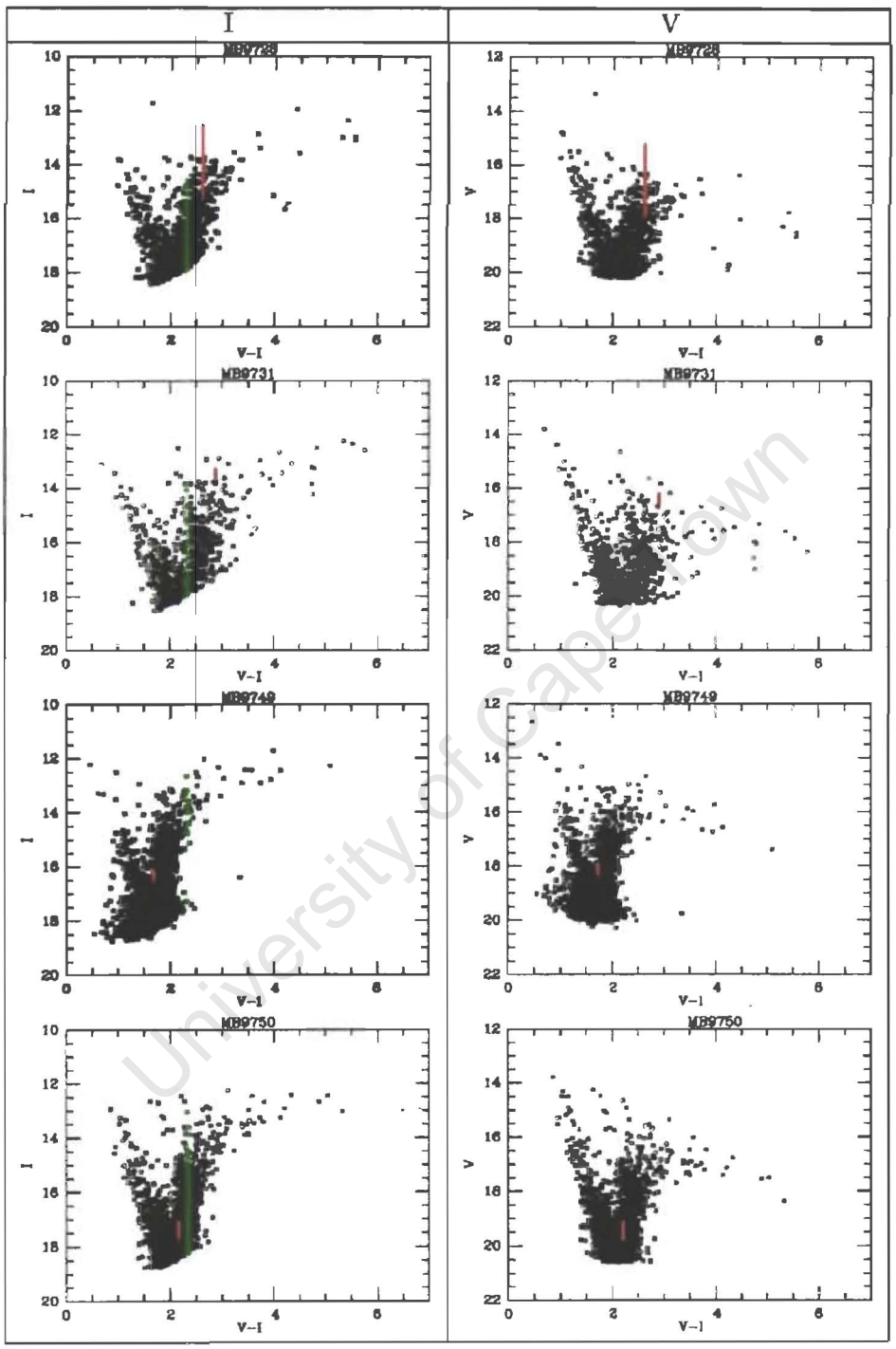

Table 8: These are the spectral types of the source stars in every observed microlensing field.

Field	Type	$(V-I)$	Sp Type	M/ $M_{\odot}$	R/ $R_{\odot}$	$D_s(kpc)$
MB9728	RGB	1.399	K2	1.12	20	7.092
MB9731	RGB	1.393	K2	1.12	20	6.318
MB9749	RGB	0.85	G2	1	8	7.44
MB9750	RGB	0.902	G5	0.92	10	7.011

Table 8 gives a breakdown of the results obtained from the spectral tables of Johnson (1966) and Landolt-Bornstein (1982). The uncertainties encountered in the calculation of $(V-I)$ could well be of the order of 0.1 mag or more, so it does not make sense to find the spectral type in any more detail. It is, however, encouraging that the spectral type for MB9728 determined here is in agreement with that determined by Albrow et al (1999), and the difference in $(V-I)$ value that they found (i.e. $V-I$ =1.14) can be attributed to their use of the more general relation used to correct the SFD map values described in Stanek (1998), which yields an extinction value of A_I =1.56 as opposed to the value 1.76 used by us in our study. This is responsible for the 0.2 magnitude difference between our $(V-I)$ value, and that of Albrow (1999). The reasons for choosing a different relation have already been discussed. Nonetheless, it is encouraging for our crude analysis that it is consistent with another study of the same event.

5.2 The Lens Masses

5.2.0 Introduction

Now, the information we have about the lensing event amounts to the following:

- The distance to the source star D_s
- The radius of the source star R_s
- . The characteristic time scale of the event given by MACHO t_o which is twice the value t_o given in equation 5.2.1.
- And the predicted maximum magnification given by MACHO $A_{\max}$.

This information can be used in the basic microlensing equations put forward (Paczynski, 1996) to try and derive the lens mass under different situations. Using the single point mass lens model (Paczynski, 1996), we can derive the mass of the lens using the equation

5.2.1 $$t_o = 0.214\text{yr}\,(\text{M}/\text{M}_\odot)^{1/2}\left(\frac{D_d}{10kpc}\right)^{\frac{1}{2}}\left(1-\frac{D_d}{D_s}\right)^{\frac{1}{2}}\left(\frac{200kms^{-1}}{V}\right)$$

where,

- D_d is the distance from the observer to the lens in kpc, and
- V is the relative transverse velocity of the lens with respect to the source in kms^{-1}.

Different values for V range between 100 and 300 kms^{-1} depending on whether the lens is located in the disk or in the bar (Zhao et al, 1995, Paczynski, 1996), while D_d is unknown. All that we do know about D_d is that it must be somewhere between the observer and the source star. For this reason, we choose a range of values for D_d so that comparison can be made.

Ranges of possible lens masses were derived using equation 5.2.1 in the following way:

- A range from D_d =1 to a value close to D_s at regular intervals of 0.5 was selected.
- The recorded timescale of the event (MACHO t_o/2) was used.
- We use the value V =200 kms^{-1} (P&S) for the transverse velocity V.
- In addition, the calculations over the range of D_d were performed for D_s (as presented in Table 8) and its upper and lower limits ($D_s \pm 0.8$ kpc) associated with the uncertainty in the distances.

As expected, the calculated lens masses were largest when the lens is very close to either the source or the observer. The derived mass will also depend on the value used for velocity. If one roughly assumes the range of possible velocities to include values between 100 kms^{-1} and 300 kms^{-1}, then the derived masses may actually change by factors of 0.25 up to 2.25 using equation 5.2.1.

5.2.1 Visibility Limits

Keeping that in mind, we looked at the possible upper limits that the lensing mass may have before it becomes bright enough to be seen (i.e. before it would become detectable by our instrument). When the light curve is modelled, one of the numbers that comes out is the blend fraction. Some of the blended light could come from the lens. If you know the apparent baseline magnitude and if it is possible to determine the contribution due to blending to be 0.05 magnitude, say, then you can find the maximum brightness of the lens from

$$10^{(-0.04*V(base+lens))} - 10^{(-0.4*V(lens))} = 10^{(0.4*(0.05))}$$

This gives V(lens) and hence M_v as before. The spectral type can then be determined if the lens is a normal dwarf.

5.2.2 Lens Equation

The following discussions of the individual events are made with reference to the range of lens masses calculated using the procedure described above. The tables are not presented here; they are inconclusive because the effects of blending (see section 5.6) have not been taken into account; rather, a brief discussion of the implications of the results is presented below.

MB9731

The lens equation, using the assumptions noted above, gives a relatively large possible lens mass. The wrong relative velocity may have been assumed. The long timescale suggests lower velocity may be more appropriate. This suggests that the lens is in the disk.

MB9749

This is a short timescale event. It is expected that most of the short time scale events occur in the Bar (Zhao et al, 1996) but this is largely a statistical assertion and is by no means the rule for microlensing models. The mass is found to be low, regardless of lens position. This suggests that the lens might be a late-type low-mass star. However, this event requires detailed modelling.

MB9750

This is a very short event (3days), resulting in extremely low mass for any position of the lens and lies in the planetary mass range. Blending may present a problem (see later section) and the event may represent a passage over a binary caustic. This system requires detailed modelling in order to get any useful information.

5.2.3 Blending

In very dense star fields the images of stars may be blended with one another. Therefore, the observed microlensing light curve can be affected by stars that aren't themselves being lensed. The blending resulting from very dense star fields may be described as follows (Han, 1997):

- When a star that is brighter than the detection limit resulting from crowding is lensed and the measured flux is affected by residual flux from other blended stars that are fainter than the detection limit.
- When one of several stars below the detection limit is lensed and its flux is associated with the flux emanating from other stars in the effective seeing disk.

In addition, the lens light can also contribute to the microlensing light curve and cause a blending effect that needs to be ascertained and taken into account in the preceding sections in order to complete the methodologies suggested for determining the mass estimates. This is beyond the scope of this thesis however and I will only include a short discussion of the effects of blending on observations instead.

The result of blending is that the microlensing optical depth is very uncertain and the Einstein timescale of events is apparently shorter. In Wozniak & Stanek (1997) a discussion of the difficulty associated with detecting the presence of a blend and correcting for it is presented. The four parameter light curve that is most often used to fit single microlensing light curves assumes that the stellar image is not blended. The use of this unblended fit to the light curve introduces a systematic bias in the estimate of event timescales and the microlensing optical depth. The even timescale t_o and the impact parameter $\mu_{\min}$ (the smallest angular distance between the source and the lens measured in units of Einstein ring radius) are affected the most and the result of neglecting blending is that (Wozniak & Stanek, 1997):

- $\mu_{\min}$ is overestimated,
- t_o is underestimated, and
- the lens mass is underestimated.

As a result of blending the observed value of maximum magnification is smaller than its true value. The errors increase with stronger blending and lower impact parameter values. Only $t_{\max}$ (the time at which maximum magnification by the lens occurs) remains well determined over a significant fraction of parameter space.

Wozniak and Stanek (1997) conclude that the presence of a blend can only be detected (using the single microlensing light curve) when the impact parameter $\mu_{\min} < 0.3$. They also mention that the red clump stars are so bright (especially in the bulge) that they would only be weakly affected by blending and due to their large angular size are more likely to be resolved by lensing.

The results presented in chapter five are speculative at best. The reason for including it was to illustrate the methodology employed and its possible usefulness. The lens mass determination is further hampered by the exclusion of the effects of blending on the microlensing light curve. The maximum mass estimates of the lenses presented in the preceding sections of 5.3 do not take

blending into account and are thus speculative at best. Any complete determination of lens masses would have to take into account the effects of blending.

5.2.4 The Minimum Detectable Mass

Seeing that the microlensing project is also concerned with the detection of planets, we would also like to investigate the lowest mass that we may be able to detect given that we have a source with a finite angular radius. This is modelled in Paczynski (1996) and the equation describing the minimum mass for which the source radius is no more than twice the projected Einstein ring radius is,

$$5.2.2 \qquad M_{\min} = 6\times10^{-8}\,\mathrm{M}_{\odot}(\mathrm{R}/\mathrm{R}_{\odot})^{2}\left(\frac{10kpc}{D_s}\right)\left(\frac{D_d}{D_s - D_d}\right).$$

In theory, one should be able to detect masses down to that of the moon in a ground based microlensing survey (Paczynski, 1996). However, to date, no planetary events have been observed in any microlensing survey, with the exception of a possible detection of a planetary object by Rhie et al (1999). Using equation 5.2.2 we derived a range of minimum detectable masses for the range of distances D_d as discussed at the beginning of section 5.2. Indeed, it depends very sensitively on how well we were able to determine its radius. The error in determining spectral type is evaluated in Table 7; the errors are small enough that at the very least, the right spectral type (i.e. K or G type) is certain. The range of source radii that is derived is not large enough to change the values presented by an order of magnitude. The minimum detectable masses (these are not presented in the text) range from masses of the order of 10^{-5} to 10^{-2} $\mathrm{M}_{\odot}$. A standard Jupiter mass object would be around 10^{-3} $\mathrm{M}_{\odot}$. Why then, if we are theoretically able to detect masses down to two orders of magnitude lower than that, are we not seeing any planetary events? Indeed, it has been asserted that 5% of all stars should have Jupiter mass planets within 5AU (Butler & Marcy, 1996)

It seems, that in order for a planetary event to become observable, there are demanding restrictions on the properties of such a binary event. The location of the planet with respect to its host star is very important. If the planet is located within the Einstein ring of the lens star then local minima would become apparent in the light curve. If the planet is located outside of the Einstein ring then

local maxima would result in the light curve. If the planet is close to the Einstein ring then the peak of the light curve is affected. The disturbances to the light curve seem to be large only for Jupiter mass planets (Paczynski, 1996). Recently it has been asserted that microlensing is more likely to be useful in the detection of planetary masses much lower than that of Jupiter (Rhie et al, 1999). It still seems that the mass fraction and the relative distance between the planet and its host star need to have values within certain tightly constrained regions in order that the planetary effect becomes observable.

5.2.5 MB9728; A Binary Event

The binary nature of the event MB9728 is investigated in Albrow (1998). The derived total mass of the lens depends upon both the radius of the source star, and the distance to the source star. Using the same approach we may derive the equations

5.5.1 $\mu = 19.17(R_*/R_\odot)\text{kms}^{-1}\text{kpc}^{-1}$

where μ is the relative lens-source proper motion and R_* is the source radius. The lens velocity v and mass can be derived using the equations below where,

5.5.2 $v = 206.8x(R_*/20R_\odot)\text{kms}^{-1}$, where $x = \frac{D_d}{D_s}$, and

5.5.3. $M = 0.179(R_*/20R_\odot)M_\odot(x/1\text{-}x)$.

Now, if the lens were located halfway to the source, the mass would be 0.179 $M_\odot$ and the velocity would be 103 kms^{-1}. If the lens were located in the Bulge, at about x=0.9, then the mass derived would be 1.611 $M_\odot$, and the velocity would be 186.12 kms^{-1}. Given that the binary mass ratio is q=0.234, we may say that if the lens is located about halfway to the source then the smaller of the components would be a brown dwarf, whereas if the lens is located in the Bulge, then the smaller

of the components is more likely to be a late M type star. This is still consistent with the findings of Albrow et al. We calculated the possible masses using equation 5.5.3 with different combinations of D_d and D_s. The conclusions drawn above are supported by our rough model calculations.

CHAPTER SIX: Brief Discussion

Our projected distance to the Galactic Centre using the E2 bar model is in close agreement with that of P&S. In addition, the roughly derived inclination of the Galactic Bar to the line of sight is in agreement with that of Stanek et al (1997). Although the uncertainty associated with the distance to each field is larger than in other studies (P&S) it is none the less in agreement with the results of the aforementioned studies that were performed utilising the red clump stars. This indication of consistency is encouraging and may reflect that we overestimate our errors. The application of the red clump distance technique is particularly suited to gravitational microlensing in view of the fact that many thousands of stars are monitored in each field. Indeed, it is easy to see how the technique could be applied with much greater accuracy by simply observing larger fields and thus more stars.

P&S achieved an uncertainty in distance of 0.3 kpc. This is encouraging for the many applications that may result from more accurate distances in microlensing, in particular, the determination of the lens mass and the spectral type of the source star. While a lens mass cannot yet be determined with absolute confidence, the distance to the field is yet one more variable with which the possible lens mass may be modelled. Its usefulness has been illustrated in chapter five and it is easy to see how the use of more accurate distances lead to a better understanding of the observed event. It is mainly the omission of the effects of blending (for which no reliable complete technique known to the author has yet been established) which limit the results of this part of our research (chapter five). A complete study of this kind is beyond the scope of this thesis, and it is the methodology that is emphasized here.

The red clump distance technique is one that has been debated at great length. It seems that no study is able to obtain a clear insight into the systematic effects that the properties of the stellar population may have on the mean magnitude of the clump. Empirical studies refute the conclusions of model-based studies. However, new projects (e.g. the multi-fibre spectrograph at the Anglo-Australian telescope) are sure to give insight into the abundances that different

populations of clump stars exhibit. This will in turn give insight into the evolutionary processes of the clump stars and the possible systematic effects on the mean clump magnitude. Given the overwhelming statistical advantages of using the red clump as a standard candle when compared to other secondary distance techniques, its use should be properly investigated as a tool in the field of gravitational microlensing. Indeed, the study conducted in this thesis has shown compatibility with that of other studies and this validates further study into the evolution of the red clump stars.

Bibliography

1. Alard, 1997, IAU Symp., 173, 215

2. Albrow, M., et al, 1998, ApJ, 509, 687

3. Albrow, M., et al, 1999, ApJ, 522, 1011

4. Alcock, C., et al, 1998, ApJ., 494, 396

5. Alves, D. R., & Sarajedini, A., 1998, ApJ, 511, 225

6. Beaulieu, J., & Sackett, P. D., 1998, AJ, 116, 209

7. Bertelli, G., et al, 1995, A&A, 301, 381

8. Bono, G., & Castellani, V., 1992, Astron. Astrophys., 258, 385

9. Butler, R.P., & Marcy, G.W., 1996, ApJ, 457, 93

10. Cannon, R.D., 1969, MNRAS, 144, 449

11. Cannon, R.D., 1970, MNRAS, 150, 111

12. Cavallo, R.M., Sweigart, A.V., & Bell, R.A., 1996, ApJ, 464, L79

13. Cavallo, R.M., Sweigart, A.V., & Bell, R.A., 1997, ApJ

14. Cole, A., 1998, ApJ, 500L, 137

15. Da Costa, G.S., & Armandroff, T.E., 1990, A.J., 100(1), 162

16. Di Stefano et al, 1995, ApJ, 448, L1

17. Dwek, E., et. al., 1995, ApJ, 445, 716

18. Freudenreich, H. T., 1998, Ap. J., 492, 495

19. Frogel, J. A., 1999, astro-ph / 9903071

20. Geisler, D., & Friel, E.D., 1992, AJ, 104,128

21. Girardi, L., et al,1998, MNRAS, 301, 1496

22. Girardi, L., 1999, submitted MNRAS, astro-ph /9901319

23. Gould, A., et al, 1997, ApJ

24. Han, C., 1997, ApJ, 490, 51

25. Harris, W.E., 1996, AJ, 112, 1487

26. Iben, I., Jnr., 1967, ARA&A, 5, 571

27. Holtzman, J., et al, 1993, AJ, 106, 1826

28. Holtzmann, J.A., et al., 1997, AJ, 113, 656

29. Jiminez, R., et al, 1995, MNRAS, 275, 1245

30. Johnson, H.L., 1966, ARA&A , 4, 193

31. Johnson, H.L., 1977, RMxAA , 2 , 175

32. Jura, M., 1987, Ap. J., 313, 743

33. Kippenhahn, R., Weigart, A., 1990, Springer-Verlag: Stellar Structure and Evolution

34. Kraft, R.P., et. al., 1993, AJ, 106, 1490

35. Kraft, R.P., et. al., 1995, AJ, 109, 2586

36. Kraft, R.P., 1994, PASP, 106, 553

37. Kraft, R.P., et. al., 1997, AJ, 113, 279

38. Landoldt-Bornstein, 1982, Vol 2b, Springer-Verlag

39. Laney, C.D., & Stobie, R.S., 1994, MNRAS, 266, 441

40. Langer, G.E., Hoffman, R.D., & Sneden, C., 1993, PASP, 105, 301

41. Langer, G.E., & Hoffman, R.D., 1995, PASP, 107, 1177

42. Mathis, J. S., 1990, Ann. Rev. Astron. Astrophys.,28, 37

43. Menzies, J.W., et. al., 1989, SAAO. Circulars, 13,1

44. Ng, Y.K., & Bertelli, G., 1996, Astron. Astrophys., 116

45. Norris, J.E., & Da Costa, G.S., 1995, ApJ, 441, L81

46. Paczynski, B., 1996, Ann. Rev. Astron. Astrophys., 34, 419

47. Paczynski, B., & Stanek,K.Z. 1998, ApJ, 494, L219

48. Paczynski, B., 1998, AcA, 48, 405

49. Reid, M.J., 1993, Ann. Rev. Astron. Astrophys., 31, 345

50. Rhie, et. al., 1999, astro-ph / 9905151

51. Schlegel, D.J., Finkbeiner, D.P.,& Davis,M., 1998, ApJ, 500, 525

52. Seidel, E., et al, 1987, Ap. J. Suppl., 63 , 917

53. Stanek, K.Z., et al, 1994, ApJ, 429, L73

54. Stanek, K. Z., 1996, Ap J, 460, L37

55. Stanek, K. Z., et al, 1998, ApJ, 500, 141

56. Stanek, K.Z., et al, 1997, ApJ, 477, 163

57. Stanek, K.Z., 1998, astro-ph/ 9802093

58. Stanek, K. Z., & Garnarvich, P. M., 1998, ApJ, 503, 131

59. Stanek, K.Z., & Garnarvich, P.M., 1998, AAS, 193, 106.5

60. Stanek, K.Z., Zaritsky, D., & Harris, J., submitted astro-ph/ 9803181

61. Sweigart, A. V.,1997, ApJ, 474, 23

62. Sweigart, A.V., & Gross, P. G., 1978, ApJ, 36, 405

63. Tayler, R.J.,1993, Cambridge University Press, Galaxies: Structure and Evolution

64. Tayler, R.J.,1994, Cambridge University Press, The Stars: their Structure and Evolution

65. Terndrup, D.M., et al, 1991, ApJ, 378, 742

66. Udalski, A., et al, 1998, AcA, 48, 1

67. Udalski, A.,1998, AcA, 48, 113

68. Udalski, A.,1998, AcA, 48, 383

69. Walker, A.R., & Terndrup, D.M., 1991, ApJ, 378, 119

70. Whitford, A. E., & Rich, R.M.,1983, ApJ, 274, 723

71. Wozniak, P.R, & Paczynski., 1997, ApJ, 487, 55

72. Wozniak, P.R, & Stanek, K.Z., 1996, ApJ, 464, 233

73. Wozniak, P.R, & Stanek, K.Z., 1997, ApJ, 487, 55-60

74. Vallenari, A., et. al., 1996, A&A, 309, 767

75. Zhao, H., et. al., 1995, ApJ, 440, L13

76. Zhao, H., et. al., 1996, MNRAS, 282, 175